

A NARROW BAND FINITE ELEMENT METHOD FOR THE LEVEL SET EQUATION

MAXIM A. OLSHANSKII ^{*}, ARNOLD REUSKEN [†], AND PAUL SCHWERING [‡]

Abstract. A finite element method is introduced to track interface evolution governed by the level set equation. The method solves for the level set indicator function in a narrow band around the interface. An extension procedure, which is essential for a narrow band level set method, is introduced based on a finite element L^2 - or H^1 -projection combined with the ghost-penalty method. This procedure is formulated as a linear variational problem in a narrow band around the surface, making it computationally efficient and suitable for rigorous error analysis. The extension method is combined with a discontinuous Galerkin space discretization and a BDF time-stepping scheme. The paper analyzes the stability and accuracy of the extension procedure and evaluates the performance of the resulting narrow band finite element method for the level set equation through numerical experiments.

1 Introduction The level set method is a widely used numerical method for the representation and approximation of moving surfaces (or interfaces) [44, 50]. The method is based on two central embeddings. The first one is the embedding of the surface as the zero level of a higher-dimensional scalar level set function, denoted by ϕ , and the second one is the embedding, or extension, of the surface’s velocity to a velocity field that transports this level set function. For a closed hypersurface $\Gamma: [0, T] \rightarrow \mathbb{R}^d$ moving with speed V_Γ in its normal direction, we consider the following *Eulerian* formulation of its evolution in a domain $\Omega \subset \mathbb{R}^d$ such that the surface is contained in Ω for all times $t \in [0, T]$:

$$\frac{\partial \phi}{\partial t} + \mathbf{u} \cdot \nabla \phi = 0, \quad (1.1)$$

where $\mathbf{u}: \Omega \rightarrow \mathbb{R}^d$ and the surface normal velocity are related by $\mathbf{u} \cdot \mathbf{n} = V_\Gamma$ on the zero level set of ϕ . Here \mathbf{n} denotes the unit normal on $\Gamma(t)$. The equation is supplemented with the initial condition $\phi(\cdot, 0) = \phi_0(\cdot)$ such that $\phi_0(x) = 0$ if and only if $x \in \Gamma(0)$.

In certain classes of applications, a canonical velocity field \mathbf{u} is given in Ω through the physics that drives the evolution of $\Gamma(t)$. A prototype example from this class is a two-phase immiscible flow problem where the evolution of the interface is driven by the continuous flow field of the two fluid phases [4, 28]. In other problem classes, the surface normal velocity is known *only* at the surface and extension velocity \mathbf{u} has to be constructed.

Our interest in the topic of this paper stems from the modeling of fluid deformable surfaces [31, 32, 42, 55]. The governing partial differential equations in such models are posed on the evolving surface $\Gamma(t)$, and the surface geometry evolution may be part of the unknown solution. An Eulerian numerical framework for this and many other interface problems, such as geometric flows, commonly utilizes a level set method for the implicit representation of the surface, while the velocity needed in the level set equation results from the surface quantities. In such a setting, the velocity field is available only on the surface or in a “small neighborhood” of it. For example, such a narrow band velocity may be provided by a TraceFEM for the spatial discretization of the surface PDE (cf. [43]). Therefore, we are interested in a finite element solver for (1.1) that is restricted to such a neighborhood of the surface, the so-called “narrow band”.

In cases where a global velocity field \mathbf{u} is known, it may also be computationally efficient to solve the level set equation (1.1) in a narrow band instead of in the whole domain Ω . These locality requirements and efficiency advantages have led to the development of narrow band level set methods, e.g., [1, 14, 15, 26, 33, 41, 58].

^{*}Department of Mathematics, University of Houston, Houston, Texas 77204-3008, USA, (maolshanskiy@uh.edu), www.math.uh.edu/~molshan

[†]Institute for Geometry and Applied Mathematics, RWTH-Aachen University, D-52056 Aachen, Germany (reusken@igpm.rwth-aachen.de)

[‡]Institute for Geometry and Applied Mathematics, RWTH-Aachen University, D-52056 Aachen, Germany (schwering@igpm.rwth-aachen.de)

1 Introduction

In this paper, we introduce a new finite element narrow band level set method based on a specific extension technique that is outlined below. For convenience, we assume that, in a narrow band, a bulk velocity \mathbf{u} is available and consider the level set equation (1.1). Narrow band methods for (1.1) require an extension procedure. To see why, assume that at time t_n we are given an approximation ϕ_h^n of $\phi(\cdot, t_n)$ in a neighborhood Ω_Γ^n of $\Gamma_h^n \approx \Gamma(t_n)$ such that we a priori know that $\Gamma_h^{n+1} \subset \Omega_\Gamma^n$; cf. Fig. 2.1. In the Eulerian setting, the numerical time integration over $[t_n, t_{n+1}]$ gives an approximation ϕ_h^{n+1} of $\phi(\cdot, t_{n+1})$ in Ω_Γ^n , which defines Γ_h^{n+1} . To be able to perform the next time step $t_{n+1} \rightarrow t_{n+2}$, the computed approximated ϕ_h^{n+1} on Ω_Γ^n has to be extended to a suitable initial value on Ω_Γ^{n+1} such that $\Gamma_h^{n+2} \subset \Omega_\Gamma^{n+1}$, and so on.

In narrow band methods known from the literature, such an extension is typically based on a level set re-initialization technique. A well-known re-initialization technique is the fast marching method (FMM), which in the context of level set method approximates the distance from a point to a given surface. The fast marching method presented in the original paper [49] is first-order accurate. Second-order accurate finite difference variants are presented in [16, 51]. A drawback of using re-initialization in level set methods is the difficulty in controlling the change of the surface position. To address this issue several finite difference-based approaches have been introduced [2, 16]. Another class of re-initialization methods involves solving an evolutionary PDE to obtain a stationary solution that satisfies the Eikonal equation [53, 54]. However, these methods have drawbacks due to parameter selection and high computational costs in a narrow band setting. An elliptic PDE-based approach [5, 58] avoids time marching to a stationary solution but requires solving a nonlinear problem and prescribing artificial boundary conditions in a narrow band. To the best of our knowledge, all these methods lack rigorous error estimates that would fit the finite element analysis of the entire narrow band discretization method.

In this paper, we present yet another approach for the extension of ϕ_h^{n+1} on Ω_Γ^n to a suitable initial value on Ω_Γ^{n+1} . The extension method proposed here is based on a finite element L^2 or H^1 projection combined with the *ghost-penalty method*. The ghost-penalty method is widely used to enhance the stability of finite element formulations [9, 10]. More recently, it was also suggested and analyzed as an implicit extension procedure for Eulerian finite element formulations of PDEs in time-dependent domains [36, 57]. We utilize the ghost-penalty in this latter capacity. The resulting extension procedure can be formulated as a *linear variational problem* in a narrow band around the surface. This makes it both computationally efficient and amenable to rigorous error analysis.

It is natural to combine this new extension method, which is variational and finite element-based, with a finite element spatial discretization for the transport equation (1.1). Discontinuous (DG) finite element methods are known to be very suitable for convection-dominated or pure transport problems, cf. e.g., [8, 12, 19, 21, 25]. We use a DG scheme from [6]. In that paper a class of DG methods for the linear level set equation (1.1) is considered and for the space semidiscrete scheme with piecewise polynomials of degree k an L^2 error bound $\mathcal{O}(h^{k+\frac{1}{2}})$ is derived, provided the solution ϕ is sufficiently smooth. The analysis of that paper applies also if the velocity field is not divergence-free. Such a DG space discretization of the level set equation (1.1) can be combined with DG in time, cf. [6]. We will use a BDF method for the discrete time integration.

The main new contribution of this paper is the particular extension method that we propose. It can be combined with any reasonable finite element based discretization method for the level set equation.

One important aspect in any narrow band level set method is the choice of suitable boundary conditions for the level set equation on the inflow boundary part of the narrow domain. The extension method that we propose has some freedom in the choice of the domains used for the local projection and for the ghost-penalty stabilization. It turns out that for an appropriate choice of these domains one can obtain higher order approximations of the zero level of ϕ , i.e., of the surface, even if the numerical boundary data have only lower order accuracy.

In this paper we do *not* use any re-initialization procedure in our narrow band level set method. It turns out that even in cases with rather large deformations of Γ we obtain reasonably accurate and stable interface

recovery without the need for re-distancing ϕ_h . In applications with (very) large deformations or in problems where an accurate approximation of the distance to Γ_h is required, one may benefit from post-processing ϕ_h^n with some standard re-distancing technique (e.g., a variant of fast marching) to obtain $\psi_h^n \simeq \text{dist}(\cdot, \Gamma_h^n)$. Using this post-processing only every k th time step, with k “large”, avoids systematic errors that could arise from using the re-distancing of ϕ_h^n in the extension procedure in every time step.

The remainder of this paper is organized as follows. In Section 2 we specify our assumptions on the level set function and explain the structure of the narrow band discretization method. In Section 3 we discuss the issue of numerical boundary conditions on the inflow boundary of the narrow band. In section 4 we explain the methods we use for spatial and time discretization of the level set equation. The main contribution of this paper is presented in Section 5. We introduce the extension method and derive accuracy bounds for it. We also present here results of numerical experiments solely for the extension method. In Section 6 we put the different ingredients together and present the complete narrow band algorithm for discretization of the level set equation. Finally, in Section 7 we demonstrate the performance of this algorithm in numerical experiments.

2 Level set equation and structure of the method We formulate the problem that we want to solve and outline the structure of our method. We assume that the evolving surface is given by the zero level of a sufficiently smooth level set function ϕ , $\Gamma(t) = \{x \in \Omega \mid \phi(x, t) = 0\}$. In a neighborhood $\mathcal{O}(\Gamma(t)) = \Omega_\epsilon(t) := \{x \in \mathbb{R}^d \mid |\phi(x, t)| < \epsilon\}$ of the surface, with fixed $\epsilon > 0$, we assume ϕ to be close to a signed distance function: For fixed constants c_1, c_2

$$0 < c_1 \leq |\nabla\phi(x, t)| \leq c_2 \quad \text{for } x \in \mathcal{O}(\Gamma(t)), t \in [0, T],$$

holds. Then the level set function is the unique solution of

$$\frac{\partial\phi}{\partial t} + \mathbf{u} \cdot \nabla\phi = 0 \quad \text{on } \bigcup_{t \in (0, T]} \mathcal{O}(\Gamma(t)) \times \{t\},$$

with a suitable initial condition $\phi(x, 0) = \phi_0(x)$ for $x \in \mathcal{O}(\Gamma(0))$. Note that we do not need inflow boundary conditions because the spatial boundary of the space-time neighborhood $\bigcup_{t \in (0, T]} \mathcal{O}(\Gamma(t)) \times \{t\}$ is a characteristic boundary. *Our primary interest is in accurately recovering $\Gamma(t)$ rather than approximating ϕ over the entire neighborhood $\bigcup_{t \in [0, T]} \mathcal{O}(\Gamma(t)) \times \{t\}$.* Therefore, it is sufficient to have an accurate approximation of ϕ on a smaller subdomain that still contains $\Gamma(t)$ for $t \in [0, T]$. This smaller domain will be specified below.

We first outline the time stepping procedure. We aim to use narrow bands Ω_Γ^n with a fixed width and a varying time step size, such that Γ^{n+1} is contained in Ω_Γ^n . The choice of the time step sizes Δt_n will be discussed later. Consider time nodes $t_n, n = 1, \dots, N$, with $0 = t_0 < t_1 < \dots < t_N = T$. We use the notations $f^n(\cdot) = f(\cdot, t_n)$ and $\Gamma^n = \Gamma(t_n)$. In the background domain Ω we assume a family of shape regular quasi-uniform simplicial triangulations $\{\mathcal{T}_h\}_{h>0}$. The subset of simplices that intersect $\Gamma(t_n)$ is denoted by $\mathcal{T}_\Gamma^n = \{T \in \mathcal{T}_h \mid \text{meas}_{d-1}(T \cap \Gamma^n) > 0\}$. To define the narrow bands used in the method, we introduce the notation for a set of neighboring elements of a sub-triangulation $\omega_h \subset \mathcal{T}_h$:

$$\mathcal{N}^1(\omega_h) := \{T \in \mathcal{T}_h \mid T \cap \omega_h \neq \emptyset\} \quad \text{and} \quad \mathcal{N}^j(\omega_h) = \mathcal{N}^1(\mathcal{N}^{j-1}(\omega_h)), \quad j \geq 2.$$

We define the narrow band $\Omega_\Gamma^n, 1 \leq n \leq N$, by adding a fixed number J of layers of elements to the “cut” elements \mathcal{T}_Γ^n :

$$\Omega_\Gamma^n = \mathcal{N}^J(\mathcal{T}_\Gamma^n). \tag{2.1}$$

Hence, for h sufficiently small we have embedding $\mathcal{T}_\Gamma^n \subset \Omega_\Gamma^n \subset \mathcal{O}(\Gamma(t_n))$. We chose the time step size Δt_n sufficiently small, such that the surface Γ^{n+1} is contained in $\Omega_\Gamma^n, n = 0, 1, \dots, N-1$, cf. Fig. 2.1 for a 1D illustration. In Section 6 we discuss how this condition is handled in our algorithm.

3 Construction of inflow boundary data

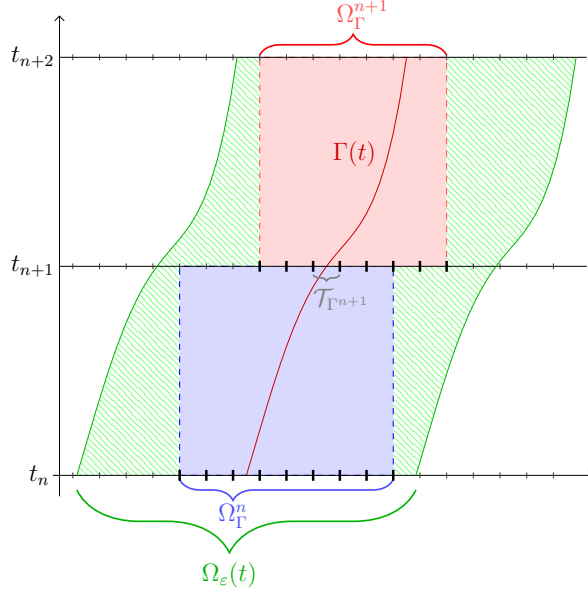


Figure 2.1: Sketch of narrow band $\mathcal{O}(\Gamma(t)) = \Omega_\epsilon(t)$ and successive time slabs $\Omega_\Gamma^n \times [t_n, t_{n+1}]$, $\Omega_\Gamma^{n+1} \times [t_{n+1}, t_{n+2}]$

In an Eulerian framework, we (approximately) solve the level set equation on a space-time subdomain $\Omega_\Gamma^n \times [t_n, t_{n+1}]$ and repeat this on the next space-time subdomain $\Omega_\Gamma^{n+1} \times [t_{n+1}, t_{n+2}]$. Clearly, for a well-posed formulation of the level set equation on $\Omega_\Gamma^n \times [t_n, t_{n+1}]$ we need initial data on Ω_Γ^n for $t = t_n$ and boundary data on the inflow part of the piecewise planar boundary of Ω_Γ^n . The inflow boundary is given by

$$\partial\Omega_{\Gamma,in}^n(t) = \{x \in \partial\Omega_\Gamma^n \mid \mathbf{u}(x, t) \cdot \mathbf{n}_{\Omega_{\Gamma^n}}(x) < 0\}, \quad t \in [t_n, t_{n+1}],$$

where $\mathbf{n}_{\Omega_{\Gamma^n}}$ denotes the outward pointing unit normal on $\partial\Omega_\Gamma^n$. For simplicity, in the remainder we assume that within each time interval the inflow boundary is constant, i.e., $\partial\Omega_{\Gamma,in}^n(t)$ is independent of $t \in [t_n, t_{n+1}]$. This inflow boundary is denoted by $\partial\Omega_{\Gamma,in}^n$. The Dirichlet boundary data on this inflow boundary are denoted by ϕ_D^n .

Given the narrow bands Ω_Γ^n , $n = 0, \dots, N-1$, that satisfy the conditions specified above, the Eulerian narrow band method that we treat in this paper has the structure outlined in Algorithm 1.

Algorithm 1 One time step structure

- a) Given ϕ_h^n , defined on Ω_Γ^n , specify boundary conditions ϕ_D^n on the inflow boundary $\partial\Omega_{\Gamma,in}^n$.
 - b) Given the initial condition ϕ_h^n and boundary data ϕ_D^n , solve the level set equation approximately on $\Omega_\Gamma^n \times [t_n, t_{n+1}]$. The result, defined on Ω_Γ^n , is denoted by $\tilde{\phi}_h^{n+1} = S(\phi_h^n, \phi_D^n)$.
 - c) Find ϕ_h^{n+1} as an extension of $\tilde{\phi}_h^{n+1}$ from Ω_Γ^n to Ω_Γ^{n+1} .
-

An approach for step a) is explained in Section 3. For solving the level set equation in step b) we apply a Galerkin DG discretization in space combined with BDF in time; see Section 4. The main new contribution of this paper is the extension method used in step c), which is explained in Section 5.

3 Construction of inflow boundary data The Dirichlet boundary data on $\partial\Omega_{\Gamma,in}^n$ will be given by a (linear) mapping $B_n : \phi_h^n \rightarrow \phi_D^n$, with $\phi_D^n = \phi_D^n(x, t)$, $x \in \partial\Omega_{\Gamma,in}^n$, $t \in [t_n, t_{n+1}]$. To define B_n , we use a straightforward approach.

One obvious possibility is to take the boundary values at time t_n ,

$$\phi_D^n = B_n \phi_h^n := (\phi_h^n)|_{\partial\Omega_{\Gamma, in}^n}, \quad (3.1)$$

i.e., we simply take the values of the approximation at $t = t_n$ restricted to the inflow boundary. These boundary data are independent of $t \in [t_n, t_{n+1}]$. If $\phi_h^n(x) = \phi(x, t_n)$ for $x \in \Omega_{\Gamma}^n$, this construction yields boundary data that are first order accurate in Δt . A second order (in time) approximation is obtained using

$$\phi_D^n = B_n(\phi_h^n, \mathbf{u}^n) := (\phi_h^n)|_{\partial\Omega_{\Gamma, in}^n} - (t - t_n)(\mathbf{u}^n \cdot \nabla \phi_h^n)|_{\partial\Omega_{\Gamma, in}^n}. \quad (3.2)$$

Both options (3.1) and (3.2) are natural choices in a BDF1 time stepping procedure. If one uses BDF2 it is natural to incorporate information of ϕ_h^{n-1} in the boundary data. Analogously to (3.1) we can use

$$\phi_D^n = B_n(\phi_h^n, \phi_h^{n-1}) := 2(\phi_h^n)|_{\partial\Omega_{\Gamma, in}^n} - (\phi_h^{n-1})|_{\partial\Omega_{\Gamma, in}^n}, \quad (3.3)$$

which is second order accurate in Δt , or a higher order approximation along the same lines as (3.2). We will discuss the choice of the boundary data in Section 7.

The default boundary data operator that we use in our numerical experiments is the one in (3.3) for BDF2. We shall discuss below in Section 6 that one can obtain higher order discretization accuracy close to the surface even if low order (in Δt) accurate Dirichlet boundary data are used. This effect is essentially caused by the transport nature of the level set problem, which implies that errors arising on a level set $|\phi(\cdot, t_n)| = ch$ do not enter the domain formed by the level sets $|\phi(\cdot, t)| < ch$ for $t \geq t_n$.

4 Discretization of the level set equation This section explains the space and time discretization that we use on one time slab $\Omega_{\Gamma}^n \times [t_n, t_{n+1}]$. We assume given Dirichlet boundary data ϕ_D^n on the inflow boundary $\partial\Omega_{\Gamma, in}^n$. To simplify the notation, we delete the time slab superscript n and write Ω_{Γ} , ϕ_h , ϕ_D instead of Ω_{Γ}^n , ϕ_h^n , ϕ_D^n in this section. We employ the discontinuous Galerkin scheme detailed in [6], paired with a BDF-scheme for the time derivative. Unlike most of the methods in the literature, this DG method does not require the velocity \mathbf{u} to be divergence-free, which is beneficial for applications that motivated this work.

We first consider the space discretization. The finite element space is given by

$$V_h^{\text{DG}}(\Omega_{\Gamma}) := \{ \psi \in L_2(\Omega_{\Gamma}) \mid \psi|_T \in P_k(T) \ \forall T \in (\mathcal{T}_h \cap \Omega_{\Gamma}) \}. \quad (4.1)$$

As is usual in DG type methods, we need the upwind fluxes and a suitable jump operator across the faces in \mathcal{T}_h . We split the boundary of an element $T \in (\mathcal{T}_h \cap \Omega_{\Gamma})$ into its inflow and outflow part

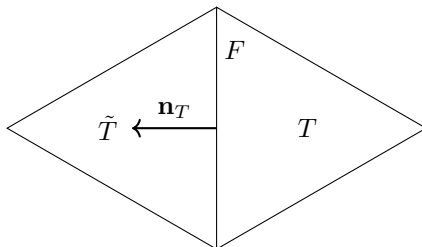
$$\partial T^-(t) := \{ x \in \partial T : \mathbf{u}(x, t) \cdot \mathbf{n}_T(x) < 0 \},$$

$$\partial T^+(t) := \{ x \in \partial T : \mathbf{u}(x, t) \cdot \mathbf{n}_T(x) \geq 0 \},$$

where \mathbf{n}_T denotes the outward pointing unit normal on T , cf. Fig. 4.1.

We introduce the jump operator $[\psi_h] = [\psi_h]|_{\partial T} = \psi_h|_T - \psi_h|_{\bar{T}}$, $\psi_h \in V_h^{\text{DG}}$. For a derivation of the following semi-discrete DG finite element method we refer to [6]: Find $\phi_h(t) \in V_h^{\text{DG}}(\Omega_{\Gamma})$ such that $\phi_h(t_n) = \phi_h^n$ and for $t \in [t_n, t_{n+1}]$:

$$\begin{aligned} \sum_{T \in (\mathcal{T}_h \cap \Omega_{\Gamma})} \left(\int_T \frac{\partial \phi_h}{\partial t} \psi_h \, \mathbf{d}\mathbf{x} + \int_T (\mathbf{u} \cdot \nabla \phi_h) \psi_h \, \mathbf{d}\mathbf{x} - \int_{\partial T \setminus \partial\Omega_{\Gamma}} [\phi_h] \psi_h (\mathbf{u} \cdot \mathbf{n}_T) \, \mathbf{d}s \right) \\ - \int_{\partial\Omega_{\Gamma, in}} \phi_h \psi_h (\mathbf{u} \cdot \mathbf{n}_{\Omega_{\Gamma}}) \, \mathbf{d}s = - \int_{\partial\Omega_{\Gamma, in}} \phi_D \psi_h (\mathbf{u} \cdot \mathbf{n}_{\Omega_{\Gamma}}) \, \mathbf{d}s \quad \text{for all } \psi_h \in V_h^{\text{DG}}(\Omega_{\Gamma}). \end{aligned} \quad (4.2)$$

Figure 4.1: Adjacent Triangles T and \tilde{T} sharing the face F .

Note that \mathbf{u} and ϕ_D may depend on t . For this formulation on a fixed polygonal domain $\Omega \subset \mathbb{R}^d$ (instead of our h dependent domain Ω_Γ), L^2 -norm error bounds of order $h^{k+\frac{1}{2}}$ are derived in [6, Theorem 3.6,3.7].

For the discretization in time, different standard approaches are known in the literature. In [6], a discontinuous Galerkin scheme in time is used. In [20, 38], a DG method in space is combined with a Runge-Kutta time discretization scheme. We opt for low-order BDF schemes for the following reasons: they necessitate only one evaluation of \mathbf{u} per time step and are easily implemented within our finite element software. Specifically, the BDF1 scheme (implicit Euler) leads to the following fully discrete problem within a single time interval: For given $\phi_h^n \in V_h^{\text{DG}}(\Omega_\Gamma^n)$, determine $\tilde{\phi}_h^{n+1} \in V_h^{\text{DG}}(\Omega_\Gamma^n)$ such that

$$\begin{aligned} & \sum_{T \in (\mathcal{T}_h \cap \Omega_\Gamma^n)} \left(\int_T \frac{\tilde{\phi}_h^{n+1} - \phi_h^n}{\Delta t_n} \psi_h \, d\mathbf{x} + \int_T (\mathbf{u}^{n+1} \cdot \nabla \tilde{\phi}_h^{n+1}) \psi_h \, d\mathbf{x} - \int_{\partial T^- \setminus \partial \Omega_\Gamma^n} [\tilde{\phi}_h^{n+1}] \psi_h (\mathbf{u}^{n+1} \cdot \mathbf{n}_T) \, ds \right) \\ & - \int_{\partial \Omega_{\Gamma, in}^n} \tilde{\phi}_h^{n+1} \psi_h (\mathbf{u}^{n+1} \cdot \mathbf{n}_{\Omega_\Gamma^n}) \, ds = - \int_{\partial \Omega_{\Gamma, in}^n} \phi_D^{n+1} \psi_h (\mathbf{u}^{n+1} \cdot \mathbf{n}_{\Omega_\Gamma^n}) \, ds \quad \text{for all } \psi_h \in V_h^{\text{DG}}(\Omega_\Gamma^n). \end{aligned} \quad (4.3)$$

The extension of this method to higher order BDF (used in the numerical experiments in Section 7) is straightforward.

REMARK 4.1. The specific choice of discretization method for the level set equation in step b) of Algorithm 1 is not crucial for the performance of our narrow band level set method. However, for the extension method discussed in the next section, it is essential to use finite element spaces. Therefore, using a finite element discretization for the level set equation is natural. Given that the level set equation is a pure transport equation, a finite element discontinuous Galerkin (DG) technique is an appropriate choice. Related DG techniques can be found in [17, 18, 52, 56]. Alternatively, a stabilized conforming finite element method, such as the streamline diffusion finite element method (cf. [47]), could be used.

In the DG method, we obtain finite element approximations that in general are discontinuous across the edges/faces of the triangulation. One variant of the extension method treated below applies to continuous H^1 conforming finite element functions. We therefore use a simple quasi-interpolation operator that maps (with optimal order of accuracy) the DG finite element functions into the H^1 conforming Lagrange finite element space with the same polynomial degree. We apply a standard Oswald interpolation in which different values of a DG finite element function around a finite element node are averaged to determine the value of the continuous finite element function at that node, cf. [29]. Using this quasi-interpolation operator in the H^1 conforming finite element space we obtain a continuous approximation $\Gamma_h(t_n)$ of the zero level $\Gamma(t_n)$.

5 Extension of the level set function In this section we propose a particular extension method for the step c) of Algorithm 1, the extension of $\tilde{\phi}_h^{n+1}$ from Ω_Γ^n to Ω_Γ^{n+1} . The proposed extension method uses a *ghost-penalty technique*. Several variants of the ghost-penalty are known in the literature. The original version,

known as local projection stabilization (LPS), was introduced in [9]. Another variant is the normal derivative jump stabilization, extensively discussed in works such as [11, 39] for its first-order version, and in [34, 48] for higher-order versions.

In our method we use the “volumetric jump” or “direct” formulation of the ghost penalty stabilization, derived in [45] and further investigated in [36, 57]. For a comparison of different ghost penalty techniques, readers are referred to [36]. In this work, we restrict ourselves to the direct formulation. To the best of our knowledge, there is no existing literature where the ghost penalty technique was applied within the framework of a narrow band level set method.

We derive and analyze the extension method in a more general setting where a function $\tilde{\phi} \in H^1(\Omega_h^p)$ is extended from a projection-subdomain $\Omega_h^p \subset \Omega$ to some extension-domain Ω_h^e such that $\Omega_h^p \subset \Omega_h^e \subset \Omega$. The result of such an extension will be a continuous finite element function ϕ_h . There is no requirement for $\tilde{\phi}$ and ϕ_h to coincide in Ω_h^p . We then apply this method for an extension from Ω_Γ^p to Ω_Γ^{p+1} in step c) of Algorithm 1, cf. Section 6.

We assume that both Ω_h^p and Ω_h^e are unions of simplices from \mathcal{T}_h . For simplicity, we identify a set of simplices with the domain defined by the union of the elements. We need some further assumption concerning the geometry of Ω_h^p and Ω_h^e . Essentially we want Ω_h^e to be an extension of the domain Ω_h^p by a few additional layers of elements. In our application, both Ω_h^p and Ω_h^e are tubular neighborhoods of width $\sim h$ around a given surface, cf. Fig. 5.1. This specific structure of Ω_h^p and Ω_h^e , however, is not needed in the analysis presented in this section. Instead, the following more general assumption is made.

ASSUMPTION 5.1. We assume that Ω_h^p consists of a subset of elements $T \in \mathcal{T}_h$ such that Ω_h^p is path-connected and such that any $T \subset \Omega_h^p$ has a common face (3D) or edge (2D) with another $T \subset \Omega_h^p$. The union of simplices Ω_h^e is such that it contains Ω_h^p and for any $T \in \Omega_h^e \setminus \Omega_h^p$ there is a path of length at most ch , with a uniform constant c , that is completely contained in Ω_h^e and connects T with an element contained in Ω_h^p .

The space of *continuous* finite element functions on a triangulated domain ω_h is denoted by

$$V_h(\omega_h) := \{\psi_h \in C(\omega_h) : \psi_h|_T \in P_k(T) \ \forall T \in \omega_h\}.$$

In the definition of the ghost-penalty stabilization below we need the difference between Ω_h^p and its extension, i.e., $\Omega_h^{\text{diff}} := \Omega_h^e \setminus \Omega_h^p$. We define the set of ghost penalty faces $\mathcal{F}_h^{\text{GP}}$ by

$$\mathcal{F}_h^{\text{GP}} := \left\{ F \subset \partial T \mid T \in \Omega_h^{\text{diff}}, F \notin \partial\Omega_h^e \right\} \cup \left\{ F \subset \partial T \mid T \in \Omega_h^p, T \cap \partial\Omega_h^e \neq \emptyset \right\}.$$

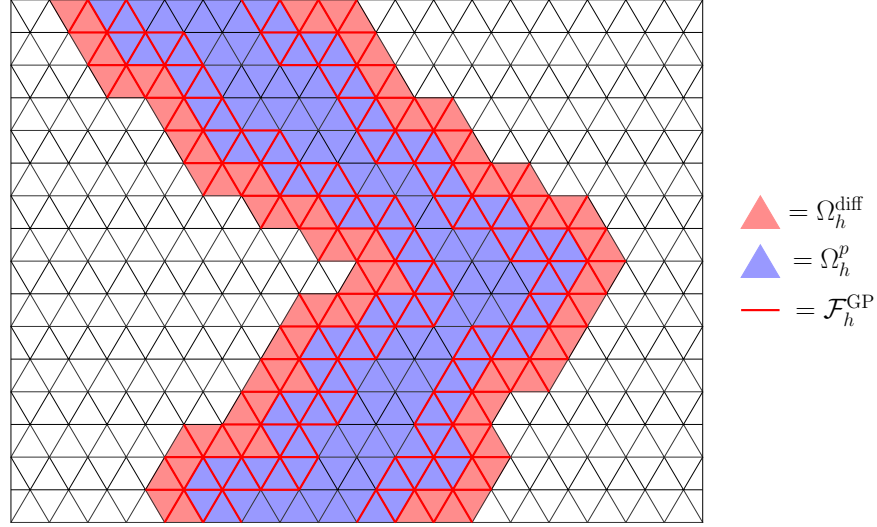
This definition ensures that all faces inside the “new” elements Ω_h^{diff} and their “inner neighbors” in Ω_h^p are included. The faces on $\partial\Omega_h^e$ are not included, since these do not have two neighboring elements in Ω_h^e . See Figure 5.1 for an illustration of Ω_h^p , Ω_h^e , and the corresponding faces $\mathcal{F}_h^{\text{GP}}$.

For a face $F = T_1 \cap T_2 \in \mathcal{F}_h^{\text{GP}}$ its corresponding patch is defined as $\omega(F) = T_1 \cup T_2$. For a finite element function $\psi \in V_h(\omega(F))$, we use the notation $\psi_i = \mathcal{E}^P \psi|_{T_i}$ with the canonical polynomial extension operator $\mathcal{E}^P : P_k(T) \rightarrow P_k(\mathbb{R}^d)$. The ghost penalty bilinear form is defined as

$$s_h^{(\alpha)}(\phi, \psi) := \gamma^{\text{ext}} h^{-\alpha} \sum_{F \in \mathcal{F}_h^{\text{GP}}} \int_{\omega(F)} (\phi_1 - \phi_2)(\psi_1 - \psi_2) \, \mathbf{d}\mathbf{x}, \quad \text{for } \phi, \psi \in V_h(\Omega_h^e), \quad (5.1)$$

with parameters $\gamma^{\text{ext}} > 0$ and α .

For the error analysis, we need the ghost penalty bilinear form $s_h^{(\alpha)}(\cdot, \cdot)$ to be well defined not only for finite element functions. We define $\psi_i = \mathcal{E}^P \Pi_{T_i} \psi|_{T_i}$ for $i = 1, 2$, where Π_{T_i} is the $L^2(T_i)$ -projection into $P_k(T_i)$, $i = 1, 2$, cf. [36]. If $\psi \in V_h(\Omega_h^e)$ it holds $\Pi_{T_i} \psi|_{T_i} = \psi|_{T_i}$. Using this, the bilinear form (5.1) is extended to $L^2(\Omega_h^e) \times L^2(\Omega_h^e)$.

Figure 5.1: Ω_h^p , Ω_h^e , and the corresponding faces $\mathcal{F}_h^{\text{GP}}$.

We now define the following bilinear forms:

$$a_h^{\text{ext}}(\phi_h, \psi_h) := (\phi_h, \psi_h)_{\Omega_h^p} + s_h^{(0)}(\phi_h, \psi_h) \quad \text{and} \quad a_{1,h}^{\text{ext}}(\phi_h, \psi_h) := (\phi_h, \psi_h)_{1, \Omega_h^p} + s_h^{(2)}(\phi_h, \psi_h),$$

with $(\cdot, \cdot)_{\Omega_h^p}$ and $(\cdot, \cdot)_{1, \Omega_h^p}$, the L^2 - and H^1 -inner product on Ω_h^p , respectively. The scaling with $\alpha = 0$ and $\alpha = 2$ in these bilinear forms is based on results from the literature.

The corresponding extension problems read: For a given function $\tilde{\phi}$ defined on Ω_h^p , determine $\phi_h \in V_h(\Omega_h^e)$ such that

$$a_h^{\text{ext}}(\phi_h, \psi_h) = (\tilde{\phi}, \psi_h)_{\Omega_h^p} \quad \text{for all } \psi_h \in V_h(\Omega_h^e), \quad (5.2a)$$

$$a_{1,h}^{\text{ext}}(\phi_h, \psi_h) = (\tilde{\phi}, \psi_h)_{1, \Omega_h^p} \quad \text{for all } \psi_h \in V_h(\Omega_h^e). \quad (5.2b)$$

In section 6 we use this extension method in the setting of the narrow band level set method, cf. component c) of the Algorithm 1. We analyze both formulations in the next section.

5.1 An error analysis of the extension. We derive error estimates for the extension methods in the L^2 - and H^1 -norm on Ω_h^e denoted by $\|\cdot\|_{\Omega_h^e}$ and $\|\cdot\|_{1, \Omega_h^e}$, respectively. It is also helpful to introduce notations for the norms $\|\cdot\|_a = \sqrt{a_h^{\text{ext}}(\cdot, \cdot)}$ and $\|\cdot\|_{1,a} = \sqrt{a_{1,h}^{\text{ext}}(\cdot, \cdot)}$.

We summarize some useful results from [36] in the following lemma.

LEMMA 5.1. *Let I_h be the Lagrange interpolation operator into the finite element space V_h . For arbitrary $\psi_h \in V_h(\Omega_h^e)$ and $\psi \in H^{k+1}(\Omega_h^e)$ there holds*

$$\|\psi_h\|_{\Omega_h^e}^2 \lesssim \|\psi_h\|_{\Omega_h^p}^2 + s_h^{(0)}(\psi_h, \psi_h), \quad (5.3)$$

$$\|\nabla \psi_h\|_{\Omega_h^e}^2 \lesssim \|\nabla \psi_h\|_{\Omega_h^p}^2 + s_h^{(2)}(\psi_h, \psi_h), \quad (5.4)$$

$$s_h^{(0)}(\psi, \psi) \lesssim h^{2k+2} \|\psi\|_{H^{k+1}(\Omega_h^e)}^2, \quad (5.5)$$

$$s_h^{(0)}(\psi - I_h \psi, \psi - I_h \psi) \lesssim h^{2k+2} \|\psi\|_{H^{k+1}(\Omega_h^e)}^2. \quad (5.6)$$

Here and below the notation $a \lesssim b$ means that the inequality $a \leq cb$ holds with a constant c which is independent of h and the position of Γ in the background mesh.

Proof. See [36, Lemma 5.2] for the proof of inequalities (5.3)–(5.4) and [36, Lemma 5.5] for the proof of inequalities (5.5)–(5.6). \square

From (5.3) and (5.4) it follows that

$$a_h^{\text{ext}}(\psi_h, \psi_h) \gtrsim \|\psi_h\|_{\Omega_h^e}^2 \quad \text{for all } \psi_h \in V_h(\Omega_h^e), \quad (5.7)$$

$$a_{1,h}^{\text{ext}}(\psi_h, \psi_h) \gtrsim \|\psi_h\|_{1,\Omega_h^e}^2 \quad \text{for all } \psi_h \in V_h(\Omega_h^e). \quad (5.8)$$

Thus, the bilinear forms $a_h^{\text{ext}}(\cdot, \cdot)$ and $a_{1,h}^{\text{ext}}(\cdot, \cdot)$ are elliptic on $V_h(\Omega_h^e)$ and the equations (5.2a) and (5.2b) are uniquely solvable.

For the error analysis we assume a $\phi \in H^{k+1}(\Omega_h^e)$, and $\tilde{\phi}$ used in (5.2) is meant to be an approximation of this ϕ on Ω_h^e . Since ϕ is defined on Ω_h^e , the error $\phi - \phi_h$ is well defined on Ω_h^e .

THEOREM 5.2. *Let $\phi \in H^{k+1}(\Omega_h^e)$ be given and $\phi_h \in V_h(\Omega_h^e)$ the solution of (5.2a). The following stability and error estimates hold*

$$\|\phi_h\|_a \leq \left(\|\tilde{\phi}\|_{\Omega_h^e}^2 - s_h^{(0)}(\phi_h, \phi_h) \right)^{\frac{1}{2}} \leq \|\tilde{\phi}\|_{\Omega_h^e} \quad (5.9)$$

$$\|\phi - \phi_h\|_{\Omega_h^e} \lesssim \|\phi - \tilde{\phi}\|_{\Omega_h^e} + h^{k+1} \|\phi\|_{H^{k+1}(\Omega_h^e)} \quad (5.10)$$

$$\|\phi - \phi_h\|_{1,\Omega_h^e} \lesssim h^{-1} \|\phi - \tilde{\phi}\|_{\Omega_h^e} + h^k \|\phi\|_{H^{k+1}(\Omega_h^e)}. \quad (5.11)$$

Proof. Let $\phi_h \in V_h(\Omega_h^e)$ be the solution of problem (5.2a). The stability estimate follows from

$$\|\phi_h\|_a^2 = a_h^{\text{ext}}(\phi_h, \phi_h) = (\tilde{\phi}, \phi_h)_{\Omega_h^e} \leq \|\tilde{\phi}\|_{\Omega_h^e} \|\phi_h\|_{\Omega_h^e} \leq \frac{1}{2} \|\tilde{\phi}\|_{\Omega_h^e}^2 + \frac{1}{2} \left(\|\phi_h\|_a^2 - s_h^{(0)}(\phi_h, \phi_h) \right).$$

Let $\hat{\phi}_h \in V_h(\Omega_h^e)$ be such that

$$a_h^{\text{ext}}(\hat{\phi}_h, \psi_h) = (\phi, \psi_h)_{\Omega_h^e} \quad \text{for all } \psi_h \in V_h(\Omega_h^e).$$

Hence, $\|\phi - \phi_h\|_{\Omega_h^e} \leq \|\phi_h - \hat{\phi}_h\|_{\Omega_h^e} + \|\phi - \hat{\phi}_h\|_{\Omega_h^e}$. We derive bounds for the two terms on the right-hand side. For the first one we use (5.7), $a_h^{\text{ext}}(\phi_h - \hat{\phi}_h, \psi_h) = (\tilde{\phi} - \phi, \psi_h)_{\Omega_h^e}$ and the stability bound yielding

$$\|\phi_h - \hat{\phi}_h\|_{\Omega_h^e} \lesssim \|\phi_h - \hat{\phi}_h\|_a \leq \|\tilde{\phi} - \phi\|_{\Omega_h^e}. \quad (5.12)$$

To bound the second term, we note that

$$\|\phi - \hat{\phi}_h\|_{\Omega_h^e} \leq \|\phi - I_h\phi\|_{\Omega_h^e} + \|I_h\phi - \hat{\phi}_h\|_{\Omega_h^e} \lesssim h^{k+1} \|\phi\|_{H^{k+1}(\Omega_h^e)} + \|I_h\phi - \hat{\phi}_h\|_{\Omega_h^e}. \quad (5.13)$$

Using

$$a_h^{\text{ext}}(\phi - \hat{\phi}_h, \psi_h) = s_h^{(0)}(\phi, \psi_h) \quad \text{for all } \psi_h \in V_h, \quad (5.14)$$

we get

$$\begin{aligned} \|I_h\phi - \hat{\phi}_h\|_a^2 &= a_h^{\text{ext}}(I_h\phi - \phi, I_h\phi - \hat{\phi}_h) + a_h^{\text{ext}}(\phi - \hat{\phi}_h, I_h\phi - \hat{\phi}_h) \\ &\stackrel{(5.14)}{=} a_h^{\text{ext}}(I_h\phi - \phi, I_h\phi - \hat{\phi}_h) + s_h^{(0)}(\phi, I_h\phi - \hat{\phi}_h) \leq \|I_h\phi - \phi\|_a \|I_h\phi - \hat{\phi}_h\|_a + \sqrt{s_h^{(0)}(\phi, \phi)} \|I_h\phi - \hat{\phi}_h\|_a. \end{aligned}$$

Reducing by $\|I_h\phi - \hat{\phi}_h\|_a$ we get

$$\|I_h\phi - \hat{\phi}_h\|_a \leq \|I_h\phi - \phi\|_a + \sqrt{s_h^{(0)}(\phi, \phi)}. \quad (5.15)$$

5 Extension of the level set function

With the help of (5.6) and (5.5) we obtain

$$\|I_h\phi - \hat{\phi}_h\|_a \leq \|I_h\phi - \phi\|_{\Omega_h^e} + \sqrt{s_h^{(0)}(I_h\phi - \phi, I_h\phi - \phi)} + \sqrt{s_h^{(0)}(\phi, \phi)} \lesssim h^{k+1}\|\phi\|_{H^{k+1}(\Omega_h^e)}. \quad (5.16)$$

Combining this estimate with the results in (5.12) and (5.13) yields the bound (5.10). For the estimate in the H^1 -norm we use the triangle inequality $\|\phi - \phi_h\|_{1, \Omega_h^e} \leq \|\phi - \hat{\phi}_h\|_{1, \Omega_h^e} + \|\hat{\phi}_h - \phi_h\|_{1, \Omega_h^e}$. For the first term we get, using an interpolation property of $I_h\phi$, a finite element inverse inequality, estimates (5.7) and (5.16),

$$\begin{aligned} \|\phi - \hat{\phi}_h\|_{1, \Omega_h^e} &\leq \|\phi - I_h\phi\|_{1, \Omega_h^e} + \|I_h\phi - \hat{\phi}_h\|_{1, \Omega_h^e} \lesssim h^k\|\phi\|_{H^{k+1}(\Omega_h^e)} + h^{-1}\|I_h\phi - \hat{\phi}_h\|_{\Omega_h^e} \\ &\lesssim h^k\|\phi\|_{H^{k+1}(\Omega_h^e)} + h^{-1}\|I_h\phi - \hat{\phi}_h\|_a \lesssim h^k\|\phi\|_{H^{k+1}(\Omega_h^e)}. \end{aligned}$$

For the second term we use (5.12):

$$\|\hat{\phi}_h - \phi_h\|_{1, \Omega_h^e} \lesssim h^{-1}\|\hat{\phi}_h - \phi_h\|_{\Omega_h^e} \lesssim h^{-1}\|\tilde{\phi} - \phi\|_{\Omega_h^e}.$$

Combining these results we get the bound (5.11). \square

Now, we give an error analysis for the extension problem (5.2b).

THEOREM 5.3. *Let $\phi \in H^{k+1}(\Omega_h^e)$ be given and $\phi_h \in V_h(\Omega_h^e)$ the solution of (5.2b). The following stability and error estimates hold*

$$\|\phi_h\|_{1, a} \leq \left(\|\tilde{\phi}\|_{1, \Omega_h^e}^2 - s_h^{(2)}(\phi_h, \phi_h) \right)^{\frac{1}{2}} \leq \|\tilde{\phi}\|_{1, \Omega_h^e} \quad (5.17)$$

$$\|\phi - \phi_h\|_{1, \Omega_h^e} \lesssim \|\phi - \tilde{\phi}\|_{1, \Omega_h^e} + h^k\|\phi\|_{H^{k+1}(\Omega_h^e)}. \quad (5.18)$$

Proof. The proof uses the same arguments as the proof of Theorem 5.2. We define $\hat{\phi}_h$ as the solution of (5.2b) with $\tilde{\phi}$ replaced by ϕ . Similar to (5.12) we obtain

$$\|\phi_h - \hat{\phi}_h\|_{1, \Omega_h^e} \lesssim \|\phi_h - \hat{\phi}_h\|_{1, a} \leq \|\tilde{\phi} - \phi\|_{1, \Omega_h^e}.$$

Applying the triangle inequality, an interpolation property of $I_h\phi$ and (5.8), we obtain the estimate:

$$\|\phi - \hat{\phi}_h\|_{1, \Omega_h^e} \leq \|\phi - I_h\phi\|_{1, \Omega_h^e} + \|I_h\phi - \hat{\phi}_h\|_{1, \Omega_h^e} \lesssim h^k\|\phi\|_{H^{k+1}(\Omega_h^e)} + \|I_h\phi - \hat{\phi}_h\|_{1, a}.$$

Repeating the estimates (5.14)–(5.15) with a_h^{ext} and $\|\cdot\|_a$ replaced by $a_{1, h}^{\text{ext}}$ and $\|\cdot\|_{1, a}$, respectively, we obtain

$$\|I_h\phi - \hat{\phi}_h\|_{1, a} \leq \|I_h\phi - \phi\|_{1, a} + \sqrt{s_h^{(2)}(\phi, \phi)}.$$

With the help of (5.5) and (5.6) we obtain

$$\begin{aligned} \|I_h\phi - \hat{\phi}_h\|_{1, a} &\leq \|I_h\phi - \phi\|_{1, \Omega_h^e} + \sqrt{s_h^{(2)}(I_h\phi - \phi, I_h\phi - \phi)} + \sqrt{s_h^{(2)}(\phi, \phi)} \\ &\leq h^k\|\phi\|_{H^{k+1}(\Omega_h^e)}, \end{aligned}$$

and so the desired estimate (5.18). \square

REMARK 5.1. We compare the results of the extension using the L^2 - and the H^1 -projection. Let $\tilde{\phi} \in V_h(\Omega_h^e)$ be a given finite element approximation of $\phi \in H^{k+1}(\Omega_h^e)$. We denote the numerical solutions of (5.2a) and (5.2b) with this $\tilde{\phi}$ by $\phi_h, \phi_{1, h} \in V_h(\Omega_h^e)$, respectively and the errors as $e_h := \tilde{\phi} - \phi_h$ and $e_{1, h} := \tilde{\phi} - \phi_{1, h}$. Note that $e_h, e_{1, h} \in V_h(\Omega_h^e)$. It holds

$$a_h^{\text{ext}}(e_h, \psi_h) = s^{(0)}(\tilde{\phi}, \psi_h) = h^2 s^{(2)}(\tilde{\phi}, \psi_h) = h^2 a_{1, h}^{\text{ext}}(e_{1, h}, \psi_h), \quad \text{for all } \psi_h \in V_h(\Omega_h^e). \quad (5.19)$$

Using an inverse inequality we get $h^2 a_{1,h}^{\text{ext}}(w_h, w_h) \leq c a_h^{\text{ext}}(w_h, w_h)$, for all $w_h \in V_h(\Omega_h^e)$. Using $\psi_h = e_h$ in (5.19) we get

$$\|e_h\|_a^2 = h^2 a_{1,h}^{\text{ext}}(e_{1,h}, e_h) \leq c \|e_{1,h}\|_a \|e_h\|_a$$

and thus $\|\tilde{\phi} - \phi_h\|_a \leq c \|\tilde{\phi} - \phi_{1,h}\|_a$ holds. Hence, measured in the energy norm $\|\cdot\|_a$, apart from a constant c , the error using the L^2 -projection is always smaller than the error using the H^1 -projection.

We present results of numerical experiments with the extension method that confirm the optimal approximation properties in section 5.3. The numerical experiments also show that there are no significant differences between the methods based on L^2 - and H^1 -projection.

5.2 Long-time behavior. We also examine another stability aspect of the extension method. Since the extension procedure is applied in *each* time step of the narrow band algorithm (cf. Section 2), it is important to assess its behavior when applied repeatedly (n times). If n is large, this provides insight into the long-term behavior of the method.

We restrict the discussion here to the L^2 -projection. Similar results hold for the method based on H^1 -projection.

For a smooth given ϕ , consider $\phi_h^0 := I_h \phi$ and define a sequence of level set function approximations $(\phi_h^n)_{n \in \mathbb{N}}$ as follows: Given $\phi_h^n \in V_h(\Omega_h^e)$ define $\phi_h^{n+1} \in V_h(\Omega_h^e)$ as the solution to the problem:

$$a_h^{\text{ex}}(\phi_h^{n+1}, \psi_h) = (\phi_h^{n+1}, \psi_h)_{\Omega_h^e} + s_h^{(0)}(\phi_h^{n+1}, \psi_h) = (\phi_h^n, \psi_h)_{\Omega_h^e} \quad \text{for all } \psi_h \in V_h(\Omega_h^e), \quad n = 0, 1, 2, \dots \quad (5.20)$$

To ease the notation we drop the subscript h below and write $\phi^n = \phi_h^n$, $s(\cdot, \cdot)$ instead of $s_h^{(0)}(\cdot, \cdot)$, and $\|\psi\|_s := s(\psi, \psi)^{\frac{1}{2}}$.

Note the following identities:

$$(\phi^{n+1} - \phi^n, \psi)_{\Omega_h^e} + s(\phi^{n+1}, \psi) = 0 \quad \text{and} \quad (\phi^n - \phi^0, \psi)_{\Omega_h^e} = - \sum_{k=1}^n s(\phi^k, \psi) \quad (5.21)$$

which hold for all $\psi \in V_h(\Omega_h^e)$. The following lemma proves two main long-time stability results

LEMMA 5.4. *The following bounds hold with a constant c independent of n and h :*

$$\|\phi^n\|_{\Omega_h^e} \leq \|\phi^0\|_{\Omega_h^e}, \quad (5.22)$$

$$\|\phi^n - \phi^0\|_{\Omega_h^e} \leq c \min\{1, \sqrt{n}h^{k+1}\} \|\phi\|_{H^{k+1}(\Omega_h^e)}. \quad (5.23)$$

Proof. Letting $\psi = \phi^{n+1}$ in (5.20) we obtain

$$\|\phi^{n+1}\|_{\Omega_h^e}^2 + \|\phi^{n+1}\|_s^2 \leq \|\phi^n\|_{\Omega_h^e} \|\phi^{n+1}\|_{\Omega_h^e} \leq \frac{1}{2} \|\phi^n\|_{\Omega_h^e}^2 + \frac{1}{2} \|\phi^{n+1}\|_{\Omega_h^e}^2,$$

which yields (5.22). If we let $\psi = \phi^{n+1} - \phi^n$ in the first identity in (5.21), we get

$$\|\phi^{n+1} - \phi^n\|_{\Omega_h^e}^2 + s(\phi^{n+1}, \phi^{n+1}) = s(\phi^{n+1}, \phi^n) \leq \frac{1}{2} \|\phi^{n+1}\|_s^2 + \frac{1}{2} \|\phi^n\|_s^2.$$

This yields $\|\phi^{n+1}\|_s \leq \|\phi^n\|_s$ and so $\|\phi^n\|_s \leq \|\phi^0\|_s$. Hence, properties (5.5) and (5.6) imply

$$\|\phi^n\|_s \leq \|\phi^0\|_s \leq \|I_h \phi - \phi\|_s + \|\phi\|_s \leq ch^{k+1} \|\phi\|_{H^{k+1}(\Omega_h^e)}. \quad (5.24)$$

Using $\psi = \phi^n - \phi^0$ in (5.21) and $\|\phi^{n+1}\|_s \leq \|\phi^n\|_s$, we get

$$\|\phi^n - \phi^0\|_{\Omega_h^e}^2 \leq n \max_{1 \leq k \leq n} \|\phi^k\|_s (\|\phi^n\|_s + \|\phi^0\|_s) \leq 2n \|\phi^0\|_s^2.$$

5 Extension of the level set function

Combining this bound with (5.24) yields (5.23) with $c\sqrt{n}h^{k+1}\|\phi\|_{H^{k+1}(\Omega_h^e)}$ at the right-hand side. This can be complemented with $\|\phi^n - \phi^0\|_{\Omega_h^p} \leq 2\|\phi^0\|_{\Omega_h^p}$, which follows from a triangle inequality and (5.22). Finally, note that $\|\phi^0\|_{\Omega_h^p} = \|I_h\phi\|_{\Omega_h^p} \leq c\|\phi\|_{H^{k+1}(\Omega_h^e)}$ holds. \square

The result in (5.23) is likely sharp in terms of dependence on n , since the initial growth of $\|\phi^n - \phi^0\|_{\Omega_h^p}$ with \sqrt{n} is observed in numerical experiments, cf. Section 5.3.

We note that the choice $\phi_h^0 := I_h\phi$ slightly simplified the analysis, but causes no loss of generality. Indeed, if $\tilde{\phi}^n$ is the sequence defined as in (5.20), with some general $\phi_h^0 = \tilde{\phi}$, then using (5.9) we obtain that $\tilde{\phi}^n$ and ϕ^n stay uniformly in n close in the following sense:

$$\|\tilde{\phi}^n - \phi^n\|_a \leq \|\tilde{\phi} - I_h\phi\|_{\Omega_h^p} \leq \|\tilde{\phi} - \phi\|_{\Omega_h^p} + ch^{k+1}\|\phi\|_{H^{k+1}(\Omega_h^e)}.$$

5.3 Numerical experiments with the extension method. We present results of numerical experiments with the ghost penalty extension method defined in (5.2). We choose the exact level set function as $\phi(\mathbf{x}) := (x_1 - x_3^2)^2 + x_2^2 + x_3^2 - 1$. The corresponding zero level defines a so-called ‘‘Kite’’-geometry, which was also used in [7, 22]. See Figure 7.1a for a visualization of the surface. The computational domain is chosen as $\Omega = [-\frac{5}{3}, \frac{5}{3}]^3$ and the initial mesh is a uniform tetrahedral mesh with mesh size $h_0 = 0.5$. In each refinement step we halve the mesh size. As in the error analysis, we use the parameter values $\alpha = 0$ for the L^2 -projection and $\alpha = 2$ for the H^1 -projection. The coefficient γ^{ext} is chosen as $\gamma^{\text{ext}} = 1$. We define the domain Ω_h^p as the elements cut by the surface, denoted by \mathcal{T}_Γ , with two layers of neighbors added, i.e., $\Omega_h^p = \mathcal{N}^2(\mathcal{T}_\Gamma)$. As the input function $\tilde{\phi}$, we take an Oswald-type interpolation of ϕ in $V_h(\Omega_h^p)$. For the polynomial degree in the finite element space V_h we consider $k = 1$ or $k = 2$. The extension elements are chosen as one and two layers of neighbors of Ω_h^p . Thus, it holds $\Omega_h^e = \mathcal{N}^1(\Omega_h^p)$ or $\Omega_h^e = \mathcal{N}^2(\Omega_h^p)$.

We investigate the L^2 - and the H^1 -errors for the L^2 - and the H^1 -projection. We present results for the errors

$$\begin{aligned} (e_{\text{ext}})^2 &:= \int_{\Omega_h^e} (\phi - \phi_h^{L^2})^2 \, d\mathbf{x}, & (e_{\text{ext}}^\nabla)^2 &:= \int_{\Omega_h^e} \nabla (\phi - \phi_h^{L^2})^2 \, d\mathbf{x}, \\ (e_{\text{ext}}^1)^2 &:= \int_{\Omega_h^e} (\phi - \phi_h^{H^1})^2 \, d\mathbf{x}, & (e_{\text{ext}}^{1,\nabla})^2 &:= \int_{\Omega_h^e} \nabla (\phi - \phi_h^{H^1})^2 \, d\mathbf{x}, \end{aligned}$$

where $\phi_h^{L^2}$ and $\phi_h^{H^1}$ denote the solutions of the ghost penalty extension using the L^2 - or the H^1 -projection, respectively. Note that the areas of the domains Ω_h^p and Ω_h^e depend on h . Therefore, for the errors we use the scaled integrals given by $\int_{\Omega_h^e} f \, d\mathbf{x} / \|1\|_{\Omega_h^e}^2$.

The results of the extension to one layer ($\Omega_h^e = \mathcal{N}^1(\Omega_h^p)$) are shown in Figure 5.2 and for two layers ($\Omega_h^e = \mathcal{N}^2(\Omega_h^p)$) in Figure 5.3. We observe convergence rates $\mathcal{O}(h^2)$ for the L^2 -error and $\mathcal{O}(h)$ for the H^1 -error in the case $k = 1$. For $k = 2$ we observe convergence rates $\mathcal{O}(h^3)$ for the L^2 -error and $\mathcal{O}(h^2)$ for the H^1 -error. These (optimal) orders of convergence are in agreement with the error analysis in Theorems 5.2 and 5.3. Note, that the errors for the L^2 -projection behave very similar to those of the H^1 -projection. In this Kite example, the exact level set function is a polynomial of degree four. Choosing $k = 4$ in the extension method leads to errors close to the machine accuracy ($\sim 10^{-11}$) for the L^2 - and the H^1 -projection.

We now consider the repeated application of the extension method, cf. Lemma 5.4 and the estimate (5.23). We start with the initial function $\phi_h^0 = I_h\phi$ and determine $\phi_h^{n+1} \in V_h(\Omega_h^e)$ such that

$$(\phi_h^{n+1}, \psi_h)_{\Omega_h^p} + s_h^{(0)}(\phi_h^{n+1}, \psi_h) = (\phi_h^n, \psi_h)_{\Omega_h^p} \quad \text{for all } \psi_h \in V_h(\Omega_h^e), \quad n = 0, 1, 2, \dots$$

holds. As in the experiments above we use the Kite-geometry and choose $\Omega_h^p = \mathcal{N}^2(\mathcal{T}_\Gamma)$ as the cut elements with two layers of neighbors added and $\Omega_h^e = \mathcal{N}^2(\Omega_h^p)$. We apply the extension method using the L^2 -projection

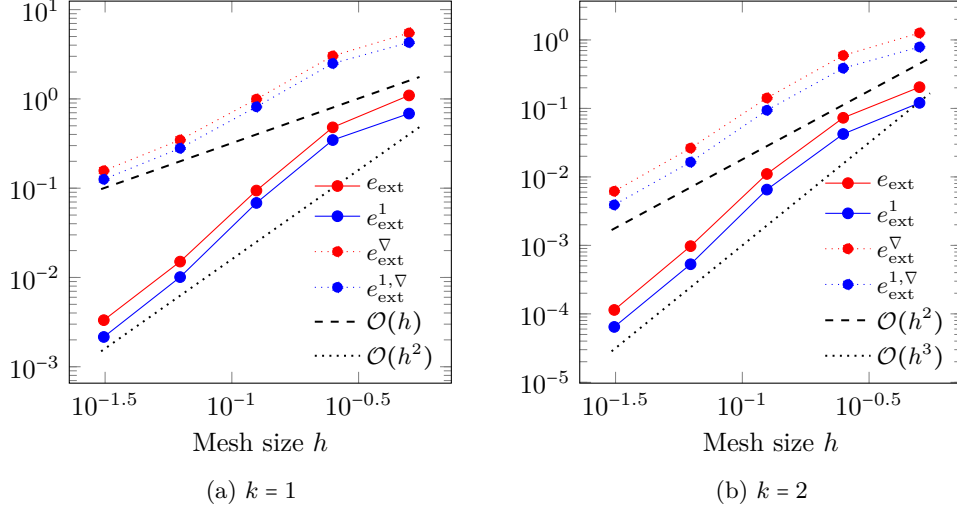


Figure 5.2: Ghost penalty extension of the level set function on one extension layer, $\Omega_h^e = \mathcal{N}^1(\Omega_h^p)$.

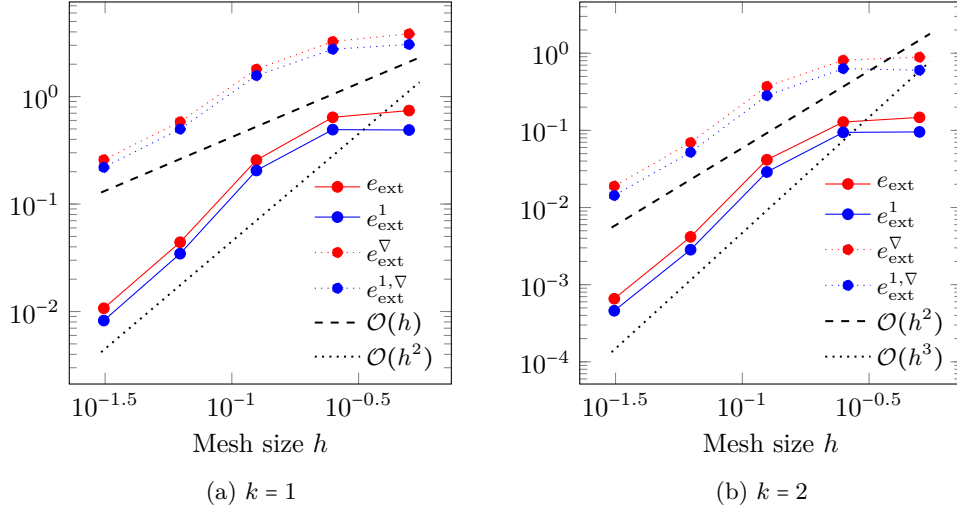


Figure 5.3: Ghost penalty extension of the level set function on two extension layers, $\Omega_h^e = \mathcal{N}^2(\Omega_h^p)$.

with $\alpha = 0$ and $\gamma^{\text{ext}} = 1$. The polynomial degrees in the finite element space are chosen as $k = 1$ and $k = 2$, and we present results for the error quantities

$$e_{\Omega_h^p} = \frac{\|\phi_h^n - \phi_h^0\|_{\Omega_h^p}}{\|1\|_{\Omega_h^p}}, \quad e_{\Omega_h^e} = \frac{\|\phi_h^n - \phi_h^0\|_{\Omega_h^e}}{\|1\|_{\Omega_h^e}},$$

The results for fixed mesh size $h = 2^{-4}$ and $0 \leq n \leq 1000$ are shown in Figure 5.4. For $k = 1$ we observe for $e_{\Omega_h^p}$ a \sqrt{n} dependence on n , consistent with (5.23). For $k = 2$ the dependence is slightly milder.

6 A level set narrow band algorithm.

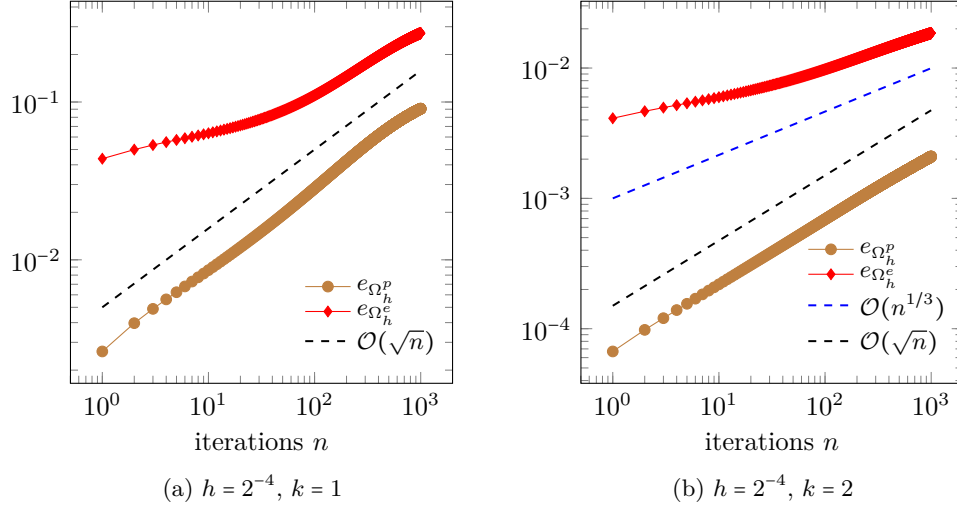


Figure 5.4: Fixed mesh size h and varying iteration number n

6 A level set narrow band algorithm. We have all ingredients ready for the narrow band level set transport as outlined in Algorithm 1. This section discusses some implementation aspects and presents more explanation on the method.

An important aspect of the method is the selection of the domains Ω_Γ^n for solving the level set equation in the time interval $[t_n, t_{n+1}]$ and the subdomain $\Omega_h^{p,n}$ where the projection in the extension method (5.2) is performed. For simplicity, we assume the velocity field \mathbf{u} is given in a sufficiently large narrow band (cf. Remark 6.1).

Recall that the domain formed by the simplices cut by Γ^n is denoted by \mathcal{T}_Γ^n . Since the exact zero level of the level set function is not available, \mathcal{T}_Γ^n is determined using the finite element approximation $\phi_h(\cdot, t_n)$ of $\phi(\cdot, t_n)$. The narrow band domain Ω_Γ^n includes \mathcal{T}_Γ^n plus a few layers of neighboring elements. In the experiments, three layers are added, so $\Omega_\Gamma^n = \mathcal{N}^3(\mathcal{T}_\Gamma^n)$. The time step is chosen so that Γ_h^{n+1} (the zero level of $\phi_h(\cdot, t_{n+1})$) is within Ω_Γ^n (see Fig. 2.1). Thus, at each time step, the level set equation is solved on a narrow band domain of width $\sim ch$, with a constant c . The level set approximation at $t = t_{n+1}$, denoted by $\tilde{\phi}_h^{n+1}$ and defined on Ω_Γ^n , is then extended to ϕ_h^{n+1} defined on Ω_Γ^{n+1} using the extension method (5.2).

Clearly the projection domain $\Omega_h^p = \Omega_h^{p,n+1}$ has to be a subdomain of both the current transport domain Ω_Γ^n where $\tilde{\phi}_h^{n+1}$ is given and the next transport domain Ω_Γ^{n+1} where ϕ_h^{n+1} has to be defined. Thus, the maximal possible projection domain is $\Omega_h^{p,n+1} = \Omega_\Gamma^n \cap \Omega_\Gamma^{n+1}$. However, we use a smaller projection domain. This choice of $\Omega_h^{p,n+1}$ addresses a key challenge in narrow band level set methods: obtaining accurate numerical boundary data on the inflow boundary. An inaccuracy of boundary data at $t = t_n$ on the inflow boundary $\partial\Omega_\Gamma^{n,in}$ can significantly affect the solution of the level set equation in $\Omega_\Gamma^n \times [t_n, t_{n+1}]$. However, due to the transport nature of the flow, such errors remain (essentially) on the same level line. For instance, an error at a point z on $\partial\Omega_\Gamma^{n,in}$ with $\phi(z, t_n) = ch$ is transported along a trajectory $z(t)$ with $\phi(z(t), t_n) = ch$ for $t \in [t_n, t_{n+1}]$. Therefore, these boundary errors do not enter the domain $\{z \in \Omega_\Gamma^n \mid |\phi(z, t_{n+1})| < ch\}$. Although this property does not hold exactly for the discrete approximation ϕ_h , it is expected to hold approximately for an accurate discretization of the level set equation.

Motivated by this observation, we use a *smaller* projection domain $\Omega_h^{p,n+1}$ than the maximal one $\Omega_\Gamma^n \cap \Omega_\Gamma^{n+1}$. Obvious candidates are \mathcal{T}_Γ^{n+1} (the domain formed by elements cut by Γ_h^{n+1}), $\mathcal{N}^1(\mathcal{T}_\Gamma^{n+1})$ (the “cut” elements and their direct neighbors), or the smallest set of simplices containing the level set h -tube $\{x \in \mathbb{R}^d \mid |\tilde{\phi}_h^{n+1}(x)| \leq$

h). In the numerical experiments, we use $\Omega_h^p = \mathcal{N}^1(\mathcal{T}_\Gamma^{n+1})$, since this domain is independent of the scaling of ϕ_h and is easy to compute. Important effects of this choice of the projection domain are illustrated in numerical experiments in Section 7.

Since we use a narrow band with a width $\sim ch$, we have to adjust the time step size to ensure that the zero level of $\phi_h(\cdot, t_{n+1})$ is within the narrow band Ω_Γ^n . The normal velocity of the surface is given by $V_\Gamma(x)$, $x \in \Gamma(t)$. Motivated by the maximal movement of the zero level set in one time step $(t_{n+1} - t_n) \max_{t \in [t_n, t_{n+1}]} \|V_\Gamma\|_{L^\infty(\Gamma(t))}$, we use the time step size $\Delta t_n = \frac{1}{2^k} \frac{(j-1)h}{2\|V_\Gamma^n\|_{L^\infty}}$. Here, k is the order of the used polynomials and j denotes the number of layers added to \mathcal{T}_Γ^n to define the narrow band. In each time step we check that the projection domain $\Omega_h^{p,n+1} = \mathcal{N}^1(\mathcal{T}_\Gamma^{n+1})$ is contained in the narrow band Ω_Γ^n . If this condition is violated, which happens only in very rare cases, we halve the time step size and redo the transport step. This procedure is repeated until the condition is satisfied.

The BDF schemes with variable time step size can be derived along the same lines as the formulas with a fix time step size. It is used and analyzed for example in [3, 13, 30, 46].

Summarizing we obtain Algorithm 2:

Algorithm 2 Narrow band level set transport

$\phi_h^0, \Omega_\Gamma^0 \leftarrow$ Initialization

while $t < T$ do:

1. $\phi_D^n \leftarrow$ determine boundary data on $\partial\Omega_{\Gamma, in}^n$, e.g. (3.3) for BDF2
 2. $\Delta t_n \leftarrow$ calculate time step size (and t_{n+1})
 3. $\tilde{\phi}_h \leftarrow$ perform transport step on $\Omega_\Gamma^n \times [t_n, t_{n+1}]$ using (4.3) and project into $V_h(\Omega_\Gamma^n)$
 4. $\Omega_\Gamma^{n+1} \leftarrow$ new narrow band with few layers around $\tilde{\Gamma}^{n+1} = \{\tilde{\phi}_h = 0\}$
 5. $\Omega_h^{p,n+1} \leftarrow \mathcal{N}^1(\mathcal{T}_\Gamma^{n+1})$
 6. if $\Omega_h^{p,n+1} \not\subset \Omega_\Gamma^n$ then $\Delta t_n \leftarrow \Delta t_n/2$ and go to step 3
 7. $\phi_h^{n+1} \leftarrow$ extension step (5.2a) of $\tilde{\phi}_h$ to Ω_Γ^{n+1}
-

Note that in this approach, we do *not* use any re-initialization of the level set function. In numerical experiments (see Section 7), we observed that for cases with smoothly evolving level sets, our approach appears to work satisfactorily even without re-initialization. An important feature of this approach is that higher-order approximations can be easily achieved by using a higher-order time and space discretization method for the level set equation and a higher-order finite element space in the extension method. Although no rigorous error analysis of the entire algorithm is available yet, rigorous error bounds for the three components (numerical boundary data, space and time discretization of the level set equation, and the extension method) that form the algorithm have been derived.

REMARK 6.1. In this paper, we assume the flow field \mathbf{u} is known in the narrow band, but this is usually not the case in practice. If the velocity field is determined by a partial differential equation on $\Gamma(t)$ and TraceFEM is used for discretization, then an approximation of the velocity field is known in a narrow band, with the width chosen in TraceFEM. In such cases, there is a strong coupling between the PDE on the surface (which determines \mathbf{u}) and the level set equation (which depends on \mathbf{u} and determines the surface location). To obtain a reasonable approximation of \mathbf{u}^{n+1} for use in (4.3), one can extrapolate the velocity in time based on previous time steps, as in [23]. If the velocity is defined in a narrow band around the surface (e.g., from TraceFEM), the extension method (5.2) can extend it to a wider band, or an implicit extension can be used as suggested in [37].

7 Numerical experiments with narrow band algorithm We give some results of numerical experiments to illustrate the performance of the narrow band level set algorithm explained in Section 6. All examples are implemented in NGSolve/netgen, cf. [40] with the add-on ngsxfem, cf. [35].

We give numerical results for the level set equation (1.1) on narrow bands in 2D and 3D. The time interval is taken as $t \in [0, 1]$ if not stated otherwise. We use the BDF2 scheme in time and first order polynomials ($k = 1$) in space or a BDF3 method combined with second order polynomials ($k = 2$). To get sufficiently good initial values for the BDF2 or BDF3 scheme, we initialize ϕ_h^0 as an interpolation of the exact level set function and start with some BDF1 time steps with a sufficiently small time step size.

In case of the BDF2 method, for the inflow boundary condition we use (3.3). If BDF3 is used, we apply an analogous time extrapolation using the values at $t \in \{t_n, t_{n-1}, t_{n-2}\}$.

If not stated otherwise, the narrow band scheme is applied on the cut elements with three layers of neighboring elements added, $\Omega_\Gamma^n := \mathcal{N}^3(\mathcal{T}_\Gamma^n)$ and for the projection domain in the extension method, we use $\Omega_h^{p,n+1} = \mathcal{N}^1(\mathcal{T}_\Gamma^{n+1})$. At each time step, we check that the projection elements for the next time step are contained in Ω_Γ^n . For the ghost penalty extension, we use the L^2 -projection with $\alpha = 0$ and $\gamma^{\text{ext}} = 1$. In each time step, the exact velocity \mathbf{u} is interpolated into a continuous finite element space of degree k on the narrow band Ω_Γ^n .

To evaluate the accuracy of the method, we track the following error metrics

$$|e_\Gamma|^2 := \sum_{n=1}^N \Delta t_n \oint_{\Gamma_h^n} (\phi^n)^2 \, d\mathbf{x}, \quad e_\Gamma^\infty = \max_{1 \leq n \leq N} \|\phi^n\|_{L^\infty(\Gamma_h^n)}, \quad |e_{L^2}|^2 := \sum_{n=1}^N \Delta t_n \oint_{\Omega_\Gamma^n} (\phi^n - \phi_h^n)^2 \, d\mathbf{x},$$

where $\|\phi^n\|_{L^\infty(\Gamma_h^n)}$ is an approximation of the maximal (absolute) value of the exact level set function ϕ^n on Γ_h^n . Recall that $\oint_{\Omega_\Gamma^n}$ stands for $|\Omega_\Gamma^n|^{-1} \int_{\Omega_\Gamma^n}$. Note, that the integrals over Γ_h^n cannot be computed exactly when using polynomials of degree $k > 1$, and standard quadrature rules cannot be applied. For this reason, we use the so-called parametric approach described for example in [27, 34] to approximate the error quantities with sufficiently high accuracy. The quantities e_Γ and e_Γ^∞ are a measure for the approximation error in $\Gamma_h^n \approx \Gamma(t_n)$.

We present results for the following test cases:

- *Deforming kite.* We consider the deformation of a kite geometry to a sphere in 3D, kite(3D), and the deformation of a kite geometry to a circle in 2D, kite(2D), cf. Figure 7.1. We present results for the error quantities for BDF2 with $k = 1$ and BDF3 with $k = 2$. Furthermore, for kite(2D) with BDF2 and $k = 1$ we illustrate the effect of different inflow boundary data.
- *Ball in a rotating flow field.* We consider a sphere (3D) or a circle (2D) that makes a full rotation, cf. Figure 7.5. We present results for the error quantities for BDF2 with $k = 1$ and BDF3 with $k = 2$. For the 2D case we show the effect of a “too large” projection domain. For the 3D case we study volume conservation properties.
- *Strongly deforming sphere.* As a more challenging and less smooth example, we consider a sphere that is stretched to a thin tube by a vortex flow field. We study different configurations and present accuracy results for BDF2 with $k = 1$ and BDF3 with $k = 2$.

7.1 Deforming kite (2D, 3D) The exact level set function of the kite is given by $\phi(x, t = 0) = (x_1 + x_2^2)^2 + x_2^2 - 1$ in 2D and $\phi(x, t = 0) = (x_1 - x_3^2)^2 + x_2^2 + x_3^2 - 1$ in 3D. We use a convex combination to deform the kite into a circle (or a sphere) with level set function $\phi(x, t = 1) = x_1^2 + x_2^2 - 1$, or $\phi(x, t) = x_1^2 + x_2^2 + x_3^2 - 1$ in 2D and 3D, respectively. The geometry evolution for the 3D case is illustrated in Figure 7.1.

The velocity field \mathbf{u} used in the level set equation has a normal component that is determined by the level set evolution: $\mathbf{u} \cdot \mathbf{n} = V_\Gamma = -\frac{\partial}{\partial t} \phi / \mathbf{n} \cdot \nabla \phi$. To illustrate that our approach is not restricted to cases with normal velocity fields, we add a tangential component \mathbf{u}_T to \mathbf{u} . We use $\mathbf{u}_T = \text{curl}_\Gamma(x_1 x_2 x_3)$ as a tangential component in 3D and the tangential component of $(y, -x)^T$ in the 2D case.

The mesh size start as $h_0 = 0.5$, and we halve it in each refinement step. The results are shown in Fig. 7.2 for the 2D case and in Fig. 7.3 for the 3D case. We observe optimal convergence rates of $\mathcal{O}(h^2)$ for $k = 1$ and $\mathcal{O}(h^3)$ for $k = 2$ for all error measures in two dimensions. In three dimensions, we observe convergence rates that are close to the optimal ones.

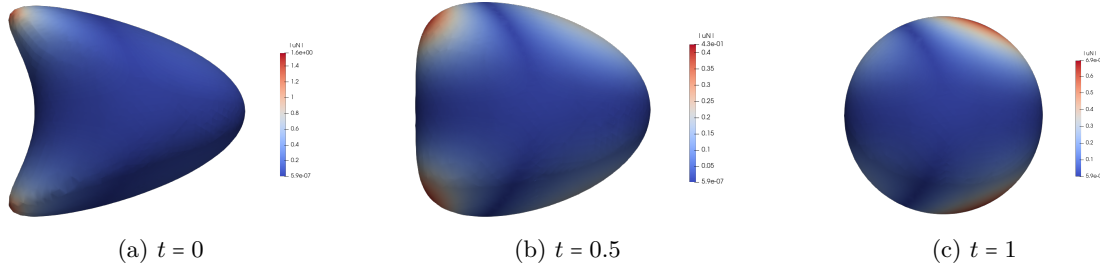


Figure 7.1: Kite deforming into a sphere.

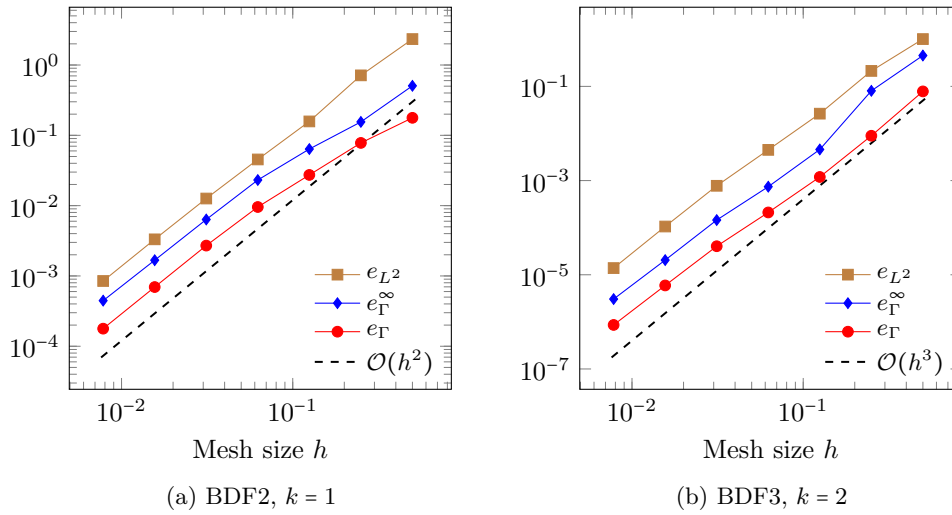


Figure 7.2: Error metrics for kite deforming to a circle in 2D

We examine the effect of the inflow boundary data, cf. Section 3. We consider `kite(2D)` with BDF2 and $k = 1$, and compare the results for the first order (in time) boundary data (3.1), the second order boundary values (3.3) and a fourth order version of the boundary data from (3.2). We determined the surface error (e_{Γ}) and the L^2 -error in the narrow band (e_{L^2}) for the three choices (low, medium and high accuracy) for boundary data. The results are shown in Figure 7.4. We observe almost no difference in the errors after the first mesh refinement. The results demonstrate that due to the choice of a suitable (sufficiently small) projection domain in the extension method we obtain higher order accuracy in the surface approximation even with low order accurate inflow boundary data.

7.2 Ball in a rotating flow field The exact level set function is given by $\phi(x, t) = (x_1 - \cos(2\pi t))^2 + (x_2 - \sin(2\pi t))^2 - \frac{1}{2}$ in 2D and $\phi(x, t) = (x_1 - \cos(2\pi t))^2 + (x_2 - \sin(2\pi t))^2 + x_3^2 - \frac{1}{2}$ in 3D. This level set function describes a sphere (or circle) that makes a full rotation around the origin for $t \in [0, 1]$. The velocity field of the rotation is given by $\mathbf{u} = 2\pi(-x_2, x_1)^T$ in 2D and $\mathbf{u} = 2\pi(-x_2, x_1, 0)^T$ in 3D. The geometry evolution is shown in Figure 7.5.

The coarsest mesh size is $h_0 = 0.25$, and we halve it in each refinement step. The results are shown in Fig. 7.6 for the 2D case and in Fig. 7.7 for the 3D case. We observe a deterioration of the convergence rate in the last refinement in the L^2 -error in the narrow band in two dimensions for $k = 2$. Recall, however, that our main

7 Numerical experiments with narrow band algorithm

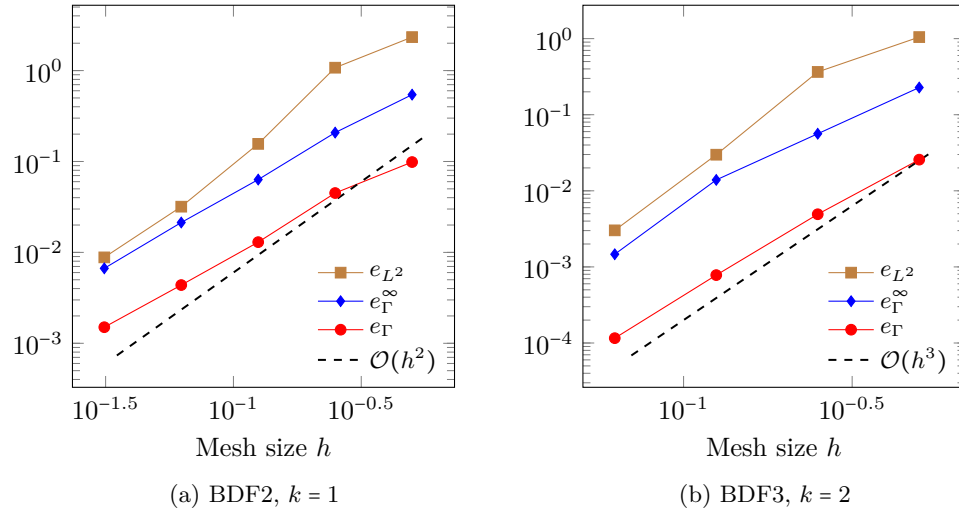


Figure 7.3: Error metrics for kite deforming to a sphere in 3D

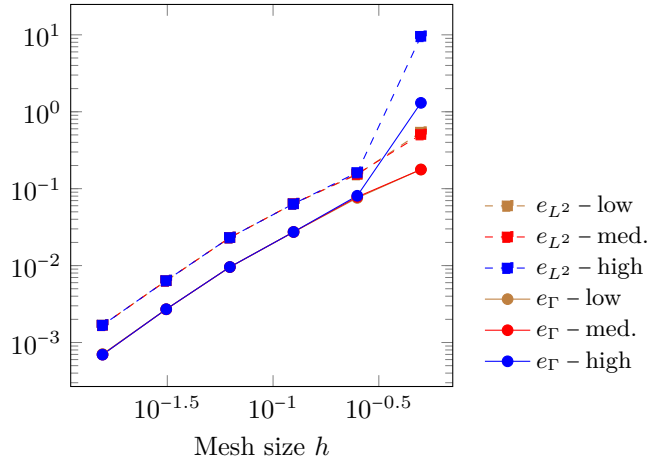


Figure 7.4: Kite deforming to a circle in 2D, BDF2, $k = 1$; different inflow boundary data

interest is in an accurate surface approximation. For this we observe optimal convergence rates of $\mathcal{O}(h^2)$ for $k = 1$ and $\mathcal{O}(h^3)$ for $k = 2$ with all corresponding error measures in two and three dimensions.

In the next experiment, we investigate how a “too large” projection domain in the ghost penalty extension method affects the accuracy of the discretization method. We compare the projection domain $\Omega_h^p = \mathcal{N}^1(\mathcal{T}_\Gamma)$, which is used in all experiments above, with the maximal possible projection domain $\Omega_h^p = \Omega_\Gamma^n \cap \Omega_\Gamma^{n+1}$. We use first order polynomials in space and a BDF2 method in time. The surface errors (L^2 - and L^∞ -errors) for the 2D case are shown in Figure 7.8. We observe that with the maximal projection domain we obtain a suboptimal rate of convergence. This confirms the heuristics discussed in Section 6.

In a further experiment, we investigate the volume conservation in 3D. Since the velocity field is divergence-free, in the continuous problem we have volume conservation. We measure the enclosed volume of the numerical approximation $\Gamma_h(t_n)$ in each time step for the lower and higher order narrow band scheme with

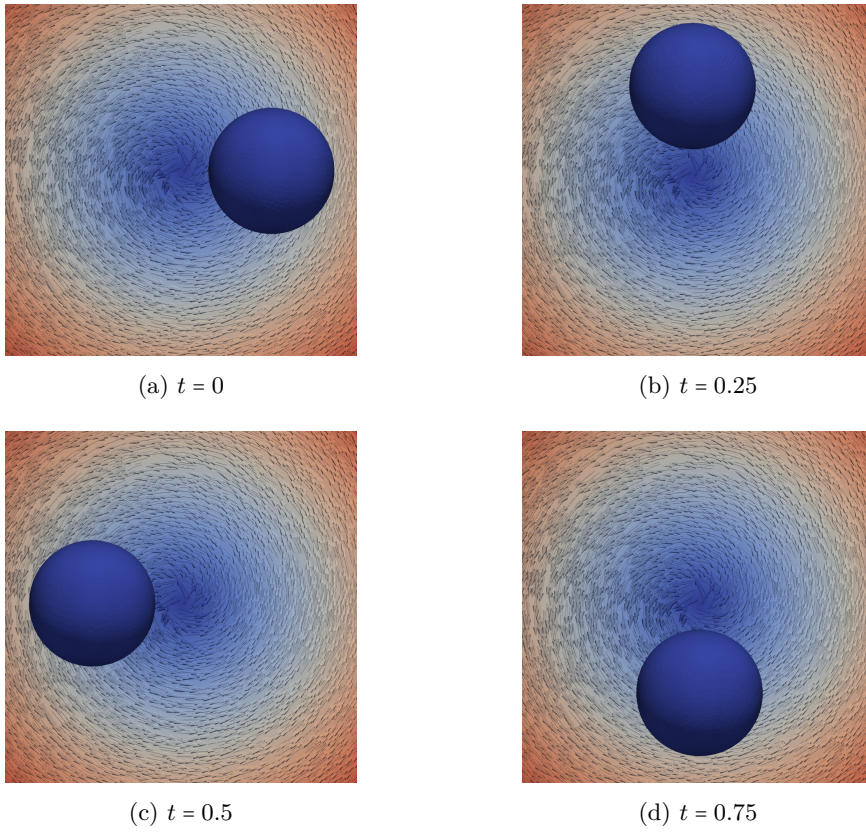


Figure 7.5: Sphere in rotating flow field

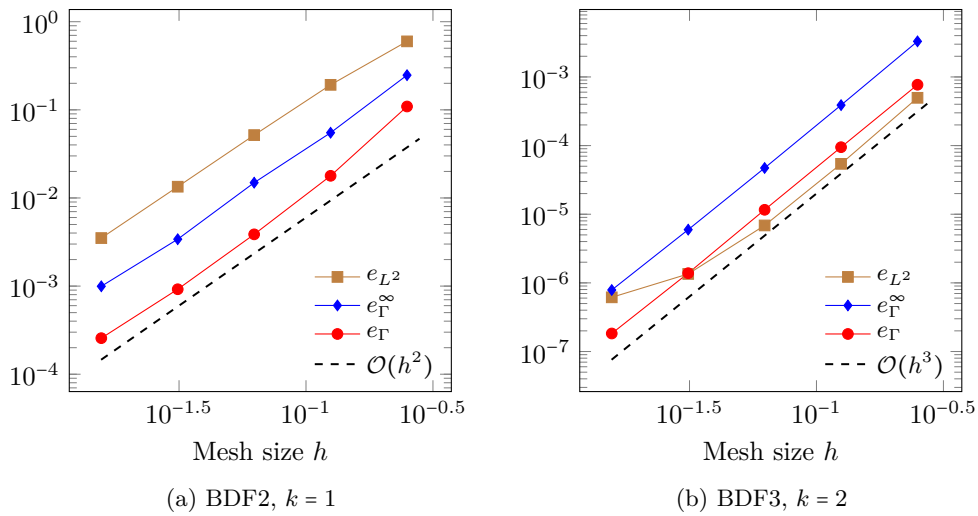


Figure 7.6: Error metrics for circle rotating around the origin in 2D

7 Numerical experiments with narrow band algorithm

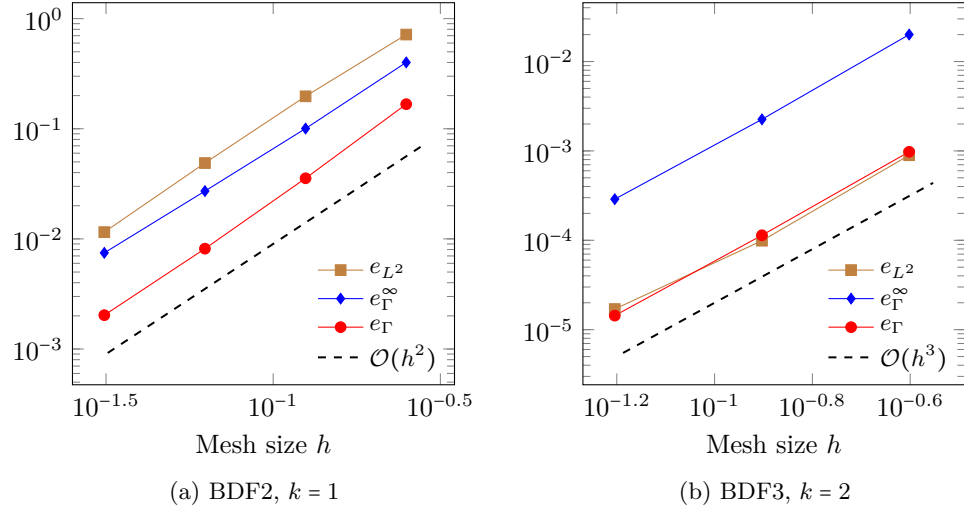


Figure 7.7: Error metrics for sphere rotating around the origin in 3D

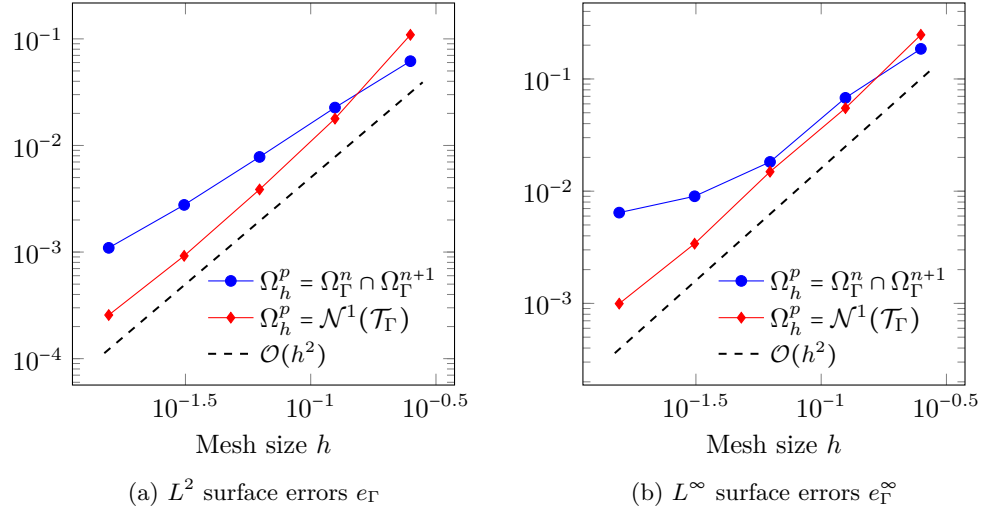


Figure 7.8: Different projection domains in extension method

fix mesh size $h = 0.0625$. The results are shown in Figure 7.9, and show that using higher order polynomials ($k = 2$), leads to a very accurate volume conservation.

7.3 Strongly deforming sphere. As an initial surface we take a sphere with radius 0.15 centered at $(0.5, 0.75, 0.5)$. A corresponding level set function is given by $\phi(x, y, z) = (x-0.5)^2 + (y-0.75)^2 + (z-0.5)^2 - 0.15^2$. The sphere is transported and deformed in a velocity field given by

$$\mathbf{u} = \cos\left(\frac{\pi}{T}t\right) \begin{pmatrix} -2 \sin(\pi x)^2 \sin(\pi y) \cos(\pi y) \\ 2 \sin(\pi y)^2 \sin(\pi x) \cos(\pi x) \\ 0 \end{pmatrix}, \quad t \in [0, T].$$

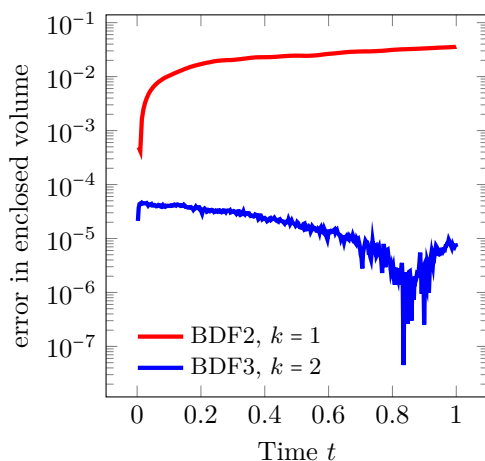


Figure 7.9: Rotating sphere; error in enclosed volume

Due to the periodic t -behaviour of this velocity field the surface will deform until $t = T/2$ and then return to the initial spherical shape at $t = T$. The surface exhibits a spiral-like deformation. Increasing T results in stronger deformed shapes of $\Gamma(t)$ at $t = T/2$. In Figure 7.10 we show resulting deformations of the sphere for $T = 2$ and $T = 4$. The maximal deformation can be observed at $t = T/2$. Similar test cases are widely used to test interface capturing and interface tracking methods, cf. [20, 24, 38].

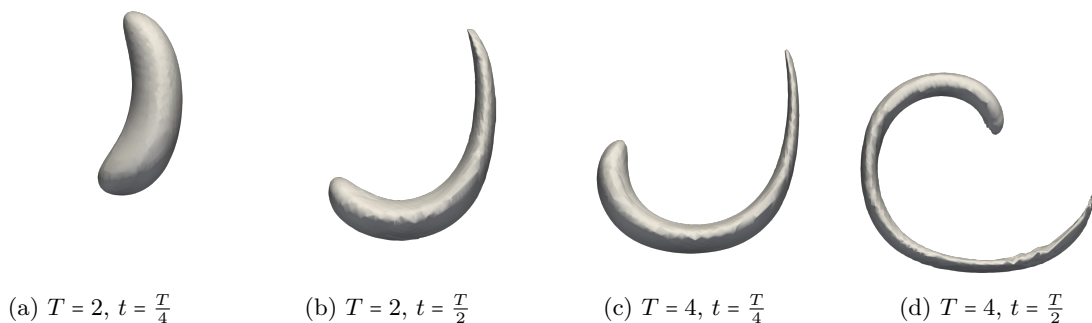


Figure 7.10: Deformations of the sphere in a vortex

We define the computational domain as $\Omega = [0, 1]^3$ and apply the transport scheme on the cut elements augmented by four layers of neighboring elements, denoted as $\Omega_{\Gamma}^n := \mathcal{N}^4(\mathcal{T}_{\Gamma}^n)$. The projection domain in the extension method consists of the cut elements with two layers of neighboring elements added, i.e. $\Omega_h^{p, n+1} = \mathcal{N}^2(\mathcal{T}_{\Gamma}^{n+1})$. We use the BDF2 and BDF3 schemes combined with finite elements of degree 1 and 2, respectively. In the previous examples, we took a variable time step size $\Delta t \sim h/\|V_{\Gamma}^n\|_{\infty}$ to ensure that the zero level of the surface remains in the transport domain Ω_{Γ}^n within the time step. However, this time step size criterion is not satisfactory in this example because the velocity V_{Γ} vanishes at $t = T/2$. Instead of a variable time step size, we take a constant time step size $\Delta t = h$ in the following experiments. At the end of each time step, we check if the zero level of the level set function stays in the transport domain. If this is not the case, the algorithm breaks down.

7 Numerical experiments with narrow band algorithm

In this example the exact level set function is not known for $t \notin \{0, T\}$. As a measure of accuracy we use

$$|e_{\Gamma, N}|^2 = \oint_{\Gamma_h(T)} \phi(\mathbf{x}, T)^2 \, d\mathbf{x},$$

which quantifies the deviation of the discrete zero level set from the spherical shape at the final time $t = T$.

We present results of our method applied to this deforming sphere example for $T = 2$ in Figure 7.11. The initial mesh and time step sizes are taken as $h_0 = \Delta t_0 = 2^{-4} = 0.0625$ and are halved in each refinement step. We observe a convergence rate of (approximately) $\mathcal{O}(h^{1.5})$ for $k = 1$ and second order convergence for $k = 2$.

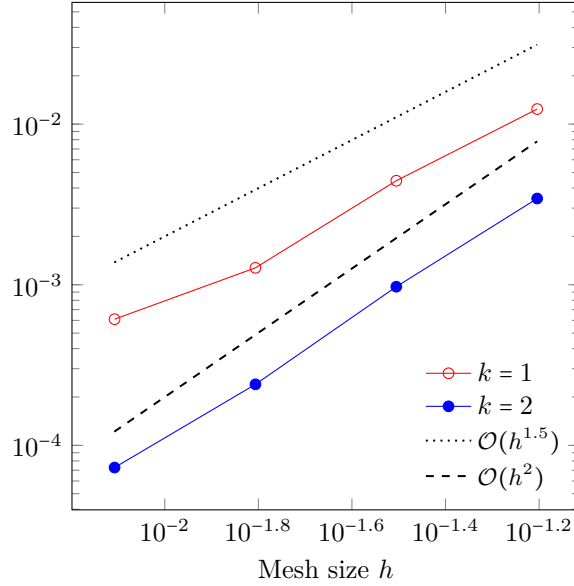


Figure 7.11: $e_{\Gamma, N}$ for $T = 2$

We show the values of $e_{\Gamma, N}$ for different end times T in Table 7.12. For certain combinations of end times T and refinement levels, we cannot report errors due to insufficient mesh resolution. By taking sufficiently small h and $k = 1$, we can handle the case $T = 4$ in which a very strong deformation occurs. For $T = 3$ and $T = 4$ we do not have results for $k = 2$ since the zero level of the level set function leaves the transport domain Ω_{Γ}^n for the given time step size $\Delta t = h$ and the algorithm breaks down. As expected, the errors are smaller for smaller T values. The convergence rates in the table vary between 1 and 2 for $k = 1$ and between 1.5 and 2.5 for $k = 2$.

h	$T = 1$				$T = 2$				$T = 3$		$T = 4$	
	$k = 1$		$k = 2$		$k = 1$		$k = 2$		$k = 1$	rate	$k = 1$	rate
	$e_{\Gamma, N}$	rate	$e_{\Gamma, N}$	rate	$e_{\Gamma, N}$	rate	$e_{\Gamma, N}$	rate	$e_{\Gamma, N}$	rate	$e_{\Gamma, N}$	rate
$6.3 \cdot 10^{-2}$	$4.2 \cdot 10^{-3}$	—	$2 \cdot 10^{-3}$	—	$1.2 \cdot 10^{-2}$	—	$3.4 \cdot 10^{-3}$	—	—	—	—	—
$3.1 \cdot 10^{-2}$	$1.5 \cdot 10^{-3}$	1.4	$3.7 \cdot 10^{-4}$	2.5	$4.4 \cdot 10^{-3}$	1.5	$9.7 \cdot 10^{-4}$	1.8	$9.9 \cdot 10^{-3}$	—	$1.6 \cdot 10^{-2}$	—
$1.6 \cdot 10^{-2}$	$4 \cdot 10^{-4}$	2	$6.3 \cdot 10^{-5}$	2.5	$1.3 \cdot 10^{-3}$	1.8	$2.4 \cdot 10^{-4}$	2	$3.1 \cdot 10^{-3}$	1.7	$6 \cdot 10^{-3}$	1.4
$7.8 \cdot 10^{-3}$	$1.3 \cdot 10^{-4}$	1.6	$1 \cdot 10^{-5}$	2.7	$6.1 \cdot 10^{-4}$	1.1	$7.3 \cdot 10^{-5}$	1.7	$1.1 \cdot 10^{-3}$	1.5	$1.9 \cdot 10^{-3}$	1.6

Figure 7.12: $e_{\Gamma, N}$ errors at final time T .

The suboptimal rates in this experiment can be explained by the rather poor mesh resolution. We do not use an adaptive mesh refinement strategy and the mesh resolution is too low to resolve the strong deformations

of the sphere. In Figure 7.13 we show a zoom of the narrow tail of the deformed sphere for $T = 4$, $t \approx T/2$ and $k = 1$. The mesh shown is for $h = 2^{-6} = 0.016$ (second refinement level). The cut elements are marked in red and the transport elements in blue. As one can see from this figure, we have a poor resolution of the part of the surface that is most strongly deformed. To overcome this problem one could use an adaptive mesh refinement strategy, which is a topic of further research. On the other hand, one may conclude that even with this relatively poor resolution we obtain fairly good results, which indicates that our method has good robustness properties with respect to strong shape deformations.

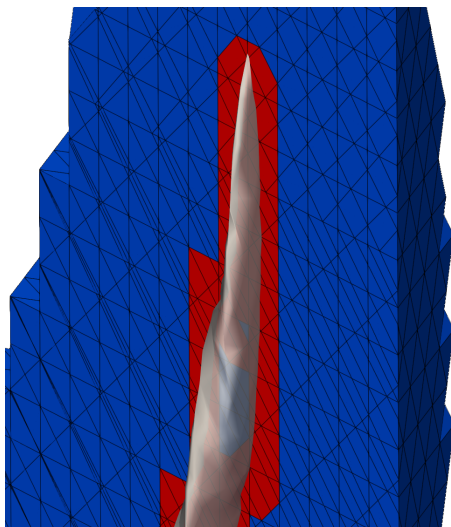


Figure 7.13: Zoom of the narrow tail of the deformed sphere, $h = 2^{-6} = 0.016$.

7.4 Conclusion A narrow-band finite element method with projection-based extension has demonstrated both effectiveness and reliability in capturing the evolution of an interface represented by the zero level of a level set function. The approach is flexible, as higher-order interface approximations can be readily achieved by selecting finite elements of higher degree and employing higher-order time integration techniques. For instance, using piecewise quadratic DG elements together with BDF3 for time integration demonstrated nearly optimal $O(h^3)$ accuracy in recovering the interface position. Interface curvatures and the normal field can be computed through straightforward elementwise calculations.

Exploiting variational properties of the projection, we have proven stability and accuracy estimates for the extension procedure. However, the error analysis of the complete method, which also involves the DG finite element formulation for the transport equation, remains an open problem for future research.

Numerical examples indicate that re-initialization of the level set function is not necessary to ensure the method's stability, even under rather large deformations of the zero level set. In applications with (very) large deformations or in problems where an accurate approximation of the distance to Γ_h is required, we recommend post-processing ϕ_h^n with some standard re-distancing technique (e.g., a variant of fast marching) to obtain $\psi_h^n \simeq \text{dist}(\cdot, \Gamma_h^n)$. Using this post-processing only every k th time step, with k “large”, avoids systematic errors that could arise from using the re-distancing of ϕ_h^n in the extension procedure in every time step.

In applications with large deformations the extension method that we propose may benefit from mesh adaptivity. This topic has not been studied, yet.

Acknowledgments: The authors A. Reusken and P. Schwering wish to thank the German Research Foundation (DFG) for financial support within the Research Unit “Vector- and tensor valued surface PDEs” (FOR 3013)

References

with project no. RE 1461/11-2. The author M. Olshanskii was partially supported by National Science Foundation under Grant No. DMS-2408978.

This material is partially based upon work supported by the National Science Foundation under Grant No. DMS-1929284 while the authors M.O. and A.R. were in residence at the Institute for Computational and Experimental Research in Mathematics in Providence, RI, during the semester program.

REFERENCES

- [1] D. ADALSTEINSSON AND J. SETHIAN, *A fast level set method for propagating interfaces*, Journal of computational physics, 118 (1995), pp. 269–277.
- [2] D. ADALSTEINSSON AND J. SETHIAN, *The fast construction of extension velocities in level set methods*, Journal of Computational Physics, 148 (1999), pp. 2 – 22.
- [3] G. AKRIVIS, M. CHEN, J. HAN, F. YU, AND Z. ZHANG, *The variable two-step bdf method for parabolic equations*, BIT Numerical Mathematics, 64 (2024).
- [4] M. ARIENTI AND M. SUSSMAN, *An embedded level set method for sharp-interface multiphase simulations of diesel injectors*, Journal of Multiphase Flow, 59 (2014), pp. 1 – 14.
- [5] C. BASTING AND D. KUZMIN, *A minimization-based finite element formulation for interface-preserving level set reinitialization*, Computing, 95 (2013), pp. 13–25.
- [6] E. BEZCHLEBOVÁ, V. DOLEJŠÍ, AND M. FEISTAUER, *Discontinuous Galerkin method for the solution of a transport level-set problem*, Computers & Mathematics with Applications, 72 (2016), pp. 455–480.
- [7] P. BRANDNER AND A. REUSKEN, *Finite element error analysis of surface Stokes equations in stream function formulation*, ESAIM: M2AN, 54 (2020), pp. 2069–2097.
- [8] F. BREZZI, L. D. MARINI, AND E. SÜLI, *Discontinuous Galerkin methods for first-order hyperbolic problems*, Mathematical Models and Methods in Applied Sciences, 14 (2004), pp. 1893–1903.
- [9] E. BURMAN, *Ghost penalty*, Comptes rendus mathématique, 348 (2010), pp. 1217–1220.
- [10] E. BURMAN, S. CLAUS, P. HANSBO, M. G. LARSON, AND A. MASSING, *Cutfem: discretizing geometry and partial differential equations*, International Journal for Numerical Methods in Engineering, 104 (2015), pp. 472–501.
- [11] E. BURMAN AND P. HANSBO, *Fictitious domain finite element methods using cut elements: II. a stabilized Nitsche method*, Applied Numerical Mathematics, 62 (2012), pp. 328–341.
- [12] E. BURMAN, A. QUARTERONI, AND B. STAMM, *Interior penalty continuous and discontinuous finite element approximations of hyperbolic equations*, Journal of Scientific Computing, 43 (2010), pp. 293–312.
- [13] G. D. BYRNE AND A. C. HINDMARSH, *Stiff ODE solvers: A review of current and coming attractions*, Journal of Computational Physics, 70 (1987), pp. 1–62.
- [14] M. H. CHO, H. G. CHOI, AND J. Y. YOO, *A direct reinitialization approach of level-set/splitting finite element method for simulating incompressible two-phase flows*, International Journal for Numerical Methods in Fluids, 67 (2011), pp. 1637–1654.
- [15] D. CHOPP, *Computing minimal surfaces via level set curvature flow*, Journal of Computational Physics, 106 (1993), pp. 77–91.
- [16] D. CHOPP, *Some improvements of the fast marching method*, SIAM J. Sci. Comput., 23 (2001), pp. 230–244.
- [17] B. COCKBURN, S. HOU, AND C.-W. SHU, *The Runge-Kutta local projection discontinuous Galerkin finite element method for conservation laws. IV: The multidimensional case*, Mathematics of Computation, 54 (1990), pp. 545–581.
- [18] B. COCKBURN AND C.-W. SHU, *TVB Runge-Kutta local projection discontinuous Galerkin finite element method for conservation laws II: General framework*, Mathematics of Computation, 52 (1989), pp. 411–435.
- [19] D. A. DI PIETRO AND A. ERN, *Mathematical Aspects of Discontinuous Galerkin Methods*, Springer Berlin Heidelberg, 2012.
- [20] D. A. DI PIETRO, S. LO FORTE, AND N. PAROLINI, *Mass preserving finite element implementations of the level set method*, Applied Numerical Mathematics, 56 (2006), pp. 1179–1195. Numerical Methods for Viscosity Solutions and Applications.
- [21] V. DOLEJŠÍ AND M. FEISTAUER, *Discontinuous Galerkin Method: Analysis and Applications to Compressible Flow*, Springer International Publishing, 2015.
- [22] G. DZIUK, *Finite elements for the Beltrami operator on arbitrary surfaces*, Hildebrandt, S., Leis, R., “Partial Differential Equations and Calculus of Variations”. Lecture Notes in Mathematics, vol 1357. Springer, Berlin, Heidelberg, (1988).
- [23] C. M. ELLIOTT, H. GARCKE, AND B. KOVÁCS, *Numerical analysis for the interaction of mean curvature flow and diffusion on closed surfaces*, Numerische Mathematik, 151 (2022), pp. 873–925.
- [24] D. ENRIGHT, R. FEDKIW, J. FERZIGER, AND I. MITCHELL, *A hybrid particle level set method for improved interface capturing*, Journal of Computational Physics, 183 (2002), pp. 83–116.
- [25] M. FEISTAUER AND K. ŠVADLENKA, *Discontinuous Galerkin method of lines for solving nonstationary singularly perturbed linear problems*, Journal of Numerical Mathematics, 12 (2004), pp. 97–117.
- [26] P. GÓMEZ, J. HERNÁNDEZ, AND J. LÓPEZ, *On the reinitialization procedure in a narrow-band locally refined level set*

- method for interfacial flows*, International journal for numerical methods in engineering, 63 (2005), pp. 1478–1512.
- [27] J. GRANDE, C. LEHRENFELD, AND A. REUSKEN, *Analysis of a high-order trace finite element method for pdes on level set surfaces*, SIAM Journal on Numerical Analysis, 56 (2018), pp. 228–255.
- [28] S. GROSS AND A. REUSKEN, *Numerical Methods for Two-phase Incompressible Flows*, Springer Berlin Heidelberg, 2011.
- [29] J.-L. GUERMOND AND A. ERN, *Finite element quasi-interpolation and best approximation*, ESAIM: Mathematical Modelling and Numerical Analysis, 51 (2017), pp. 1367 – 1385.
- [30] E. HAIRER AND G. WANNER, *Solving Ordinary Differential Equations II*, Springer Berlin Heidelberg, 1996.
- [31] D. HU, P. ZHANG, AND E. WEINAN, *Continuum theory of a moving membrane*, Physical Review E, 75 (2007), p. 041605.
- [32] T. JANKUHN, M. OLSHANSKII, AND A. REUSKEN, *Incompressible fluid problems on embedded surfaces: modeling and variational formulations*, Interfaces and Free Boundaries, 20 (2018), pp. 353–377.
- [33] C. LEE, J. DOLBOW, AND P. J. MUCHA, *A narrow-band gradient-augmented level set method for multiphase incompressible flow*, Journal of Computational Physics, 273 (2014), pp. 12–37.
- [34] C. LEHRENFELD, *A higher order isoparametric fictitious domain method for level set domains*, in Geometrically Unfitted Finite Element Methods and Applications, S. P. A. Bordas, E. Burman, M. G. Larson, and M. A. Olshanskii, eds., Springer International Publishing, 2017, pp. 65–92.
- [35] C. LEHRENFELD, F. HEIMANN, J. PREUSS, AND H. VON WAHL, *ngsxfem: Add-on to ngsolve for geometrically unfitted finite element discretizations*. Journal of Open Source Software, 6(64), 3237,.
- [36] C. LEHRENFELD AND M. OLSHANSKII, *An Eulerian finite element method for pdes in time-dependent domains*, ESAIM: M2AN, 53 (2019), pp. 585–614.
- [37] C. LEHRENFELD, M. OLSHANSKII, AND X. XU, *A stabilized trace finite element method for partial differential equations on evolving surfaces*, SIAM Journal on Numerical Analysis, 56 (2018), pp. 1643–1672.
- [38] E. MARCHANDISE, J.-F. REMACLE, AND N. CHEVAUGEON, *A quadrature-free discontinuous Galerkin method for the level set equation*, Journal of Computational Physics, 212 (2006), pp. 338–357.
- [39] A. MASSING, M. G. LARSON, A. LOGG, AND M. E. ROGNES, *A stabilized Nitsche fictitious domain method for the Stokes problem*, Journal of Scientific Computing, 61 (2014), pp. 604–628.
- [40] NETGEN/SOLVE. <https://ngsolve.org/>.
- [41] L. C. NGO AND H. G. CHOI, *Efficient direct re-initialization approach of a level set method for unstructured meshes*, Computers & Fluids, 154 (2017), pp. 167–183.
- [42] I. NITSCHKE, S. REUTHER, AND A. VOIGT, *Hydrodynamic interactions in polar liquid crystals on evolving surfaces*, Physical Review Fluids, 4 (2019), p. 044002.
- [43] M. OLSHANSKII, A. REUSKEN, AND P. SCHWERING, *An eulerian finite element method for tangential navier-stokes equations on evolving surfaces*, Mathematics of Computation, 93 (2024), pp. 2031–2065.
- [44] S. OSHER, R. FEDKIW, AND K. PIECHOR, *Level set methods and dynamic implicit surfaces*, Appl. Mech. Rev., 57 (2004), pp. B15–B15.
- [45] J. PREUSS, *Higher order unfitted isoparametric space-time FEM on moving domains*, mathesis, Institute for Numerical and Applied Mathematics University of Göttingen, 02 2018.
- [46] G. K. ROCKSWOLD, *Stable variable step stiff methods for ordinary differential equations*, PhD thesis, Iowa State University, 1983.
- [47] H.-G. ROOS, M. STYNES, AND L. TOBISKA, *Robust Numerical Methods for Singularly Perturbed Differential Equations*, Springer Berlin Heidelberg, 2008.
- [48] B. SCHOTT AND W. A. WALL, *A new face-oriented stabilized XFEM approach for 2D and 3D incompressible Navier–Stokes equations*, Computer Methods in Applied Mechanics and Engineering, 276 (2014), pp. 233–265.
- [49] J. A. SETHIAN, *A fast marching level set method for monotonically advancing fronts*, Proceedings of the National Academy of Sciences of the United States of America, 93 (1996), pp. 1591–1595.
- [50] ———, *Theory, algorithms, and applications of level set methods for propagating interfaces*, Acta Numerica, 5 (1996), pp. 309–395.
- [51] ———, *Fast marching methods*, SIAM Review, 41 (1999), pp. 199–235.
- [52] J. SUDIRHAM, J. VAN DER VEGT, AND R. VAN DAMME, *Space-time discontinuous Galerkin method for advection-diffusion problems on time-dependent domains*, Applied Numerical Mathematics, 56 (2006), pp. 1491–1518.
- [53] M. SUSSMAN AND E. FATEMI, *An efficient interface preserving level set redistancing algorithm and its application to interfacial incompressible fluid flow*, SIAM J. Sci. Comp., 20 (1999), pp. 1165 – 1191.
- [54] A.-K. TORNBERG AND B. ENGQUIST, *A finite element based level-set method for multiphase flow applications*, Comp. Vis. Sci., 3 (2000), pp. 93–101.
- [55] A. TORRES-SÁNCHEZ, D. MILLÁN, AND M. ARROYO, *Modelling fluid deformable surfaces with an emphasis on biological interfaces*, Journal of fluid mechanics, 872 (2019), pp. 218–271.
- [56] J. VAN DER VEGT AND J. SUDIRHAM, *A space-time discontinuous Galerkin method for the time-dependent Oseen equations*, Applied Numerical Mathematics, 58 (2008), pp. 1892–1917. Special Issue in Honor of Piet Hemker.
- [57] H. VON WAHL, T. RICHTER, AND C. LEHRENFELD, *An unfitted Eulerian finite element method for the time-dependent Stokes problem on moving domains*, IMA Journal of Numerical Analysis, 42 (2022), pp. 2505–2544.
- [58] T. XUE, W. SUN, S. ADRIAENSSENS, Y. WEI, AND C. LIU, *A new finite element level set reinitialization method based on the shifted boundary method*, Journal of Computational Physics, 438 (2021), p. 110360.